Functional Analysis of RIG-I and RNP Complexes in the Antiviral Interferon System

Oh Seong-Wook

Contents

Abstract

RIG-I is a crucial cytosolic viral RNA sensor that triggers signal transduction to induce the antiviral cytokine, interferon (IFN). RIG-I selectively recognizes non-self signatures of viral RNA, such as 5'-triphosphate and double-stranded RNA. However, the spatiotemporal dynamics of RIG-I recognition and its signaling remain elusive. In this study, I intensively investigated the time-course of events in cells infected with NDV, a negative-single-stranded RNA virus of *Mononegavirales*, especially focusing on the correlation between the action of RIG-I and the kinetics of IFN induction.

In the early phase of NDV infection, formation of viral replication complexs (vRCs) consisting of viral proteins and RNAs was observed, and RIG-I accumulated in vRCs to induce primary IFN. In the late phase, host antiviral stress granules (avSGs) were also induced beside vRCs, and RIG-I was also distributed to avSGs. Interestingly, only positive-strand poly(A)$^+$ viral RNA migrated to avSGs among viral RNAs in vRCs. Inhibition of avSGs considerably impaired the magnitude of IFN upon viral infection, suggesting that avSG-associated RIG-I was responsible for the secondary amplification of IFN. I further identified uncapped poly(A)$^+$ viral RNA covering leader and N gene derived from read-through transcription of NDV as the responsible ligand for RIG-I activation. Intriguingly, production of this read-through RNA was not limited to NDV but commonly observed in other *Mononegavirales* viruses, RSV and VSV.

Taken together, this study demonstrates that the clusters of RNP complexes; vRCs and avSGs are locales where RIG-I encounters viral RNAs to trigger primary induction and secondary amplification of IFN, and identifies a viral read-through transcript as a novel natural ligand of RIG-I.

1. Introduction

1-1. The innate immunity

Higher animals, including humans, have developed a self-defense system against infection by pathogenic microbes such as fungi, parasites, bacteria, and viruses. The system consists of two principal processes; “innate immunity” and “adaptive immunity”, both of which are indispensable for controlling cellular responses against infection. The innate immunity, in particular, governs rapid clearance of invading pathogens immediately after infection. Therefore, how animals build this “first barrier of defense” against infection is a critical determinant of their fate. Pathogens, on the other hand, have evolved to subvert the host’s barrier by disrupting key components of the defense system for their successful survival, indicating the prominent role of the innate immunity on host-pathogen interaction.

The greatest advance in the study of the innate immunity was the discovery of host pattern recognition receptors (PRRs), which detect a diverse range of conserved pathogen-specific structures referred to as pathogen-associated molecular patterns (PAMPs) [1]. Based on genetic and functional relationships, PRRs are now classified into four large groups; Toll-like receptors (TLRs), C-type lectin receptors (CLRs), nucleotide-binding oligomerization domain (NOD)-like receptors (NLRs), and retinoic acid-inducible gene I (RIG-I)-like receptors (RLRs). TLRs were first identified as a human homolog of the *Drosophila* Toll protein, and now 10 human TLR family members, which are all expressed either on the cell membrane or on the endosomes of immunocompetent cells such as macrophages and dendritic cells, have been

characterized [1]. TLRs encounter PAMPs exclusively in the extracellular compartment and elicit multiple cellular programs including inflammation, apoptosis, and stimulation of downstream adaptive immunity. CLRs are also known as transmembrane PRR, which plays more important role in antifungal innate immunity.

Meanwhile, PAMPs exposed in the cytoplasm should be detected by other intracellular PRRs. NLRs, which are composed of 22 members in humans, are specialized PRRs for bacterial PAMPs recognition leading to activation of inflammatory and apoptotic responses. Intracellular recognition of viral single-stranded RNA (ssRNA) and double-stranded RNA (dsRNA) is mediated by RLRs, which consist of three RNA helicases including RIG-I, MDA5, and LGP2. RIG-I and MDA5 have been demonstrated to directly bind to a variety of viral RNA species and trigger a signaling cascade to induce production of antiviral cytokine termed interferon (IFN). TLRs, NLRs, CLRs, and RLRs are all critical PRRs that synergistically drive the innate immune responses against microbial infection [2].

1-2. RIG-I-like receptors

1-2-1. Structure

Retinoic acid-inducible gene I (RIG-I), which is encoded by the *DDX58* gene, is the DExD/H-box RNA helicase expressed in the cytoplasm. RIG-I was first identified as a crucial sensor molecule that detects viral infection and induces an important antiviral cytokine, Type I IFN (IFN-α/β) [3]. RIG-I consists of three functional domains; N-terminal tandem caspase activation and recruit domains (CARDs), intermediate

DExD/H-box RNA helicase domain, and C-terminal domain (CTD) (Figure 1-1). The helicase domain includes an ATP-binding site, which is essential for the helicase/ATPase activity that drives RIG-I. RIG-I shares similar domain structures and functional properties with melanoma differentiation-associated gene 5 (MDA5) and laboratory of genetics and physiology 2 (LGP2), which thereby gathers these proteins into a family of RNA helicases referred to as RIG-I-like receptors (RLRs) (Figure 1-1). RLRs are found only in the higher vertebrates, and are ubiquitously expressed in most tissues. Among RLRs, RIG-I and MDA5 equip all three functional domains and are defined as positive regulators of antiviral response. On the other hand, since LGP2 lacks the CARDs, it is supposed to play distinct roles in RLR signaling (see below).

1-2-2. Signaling

In a steady state without viral infection, RIG-I is kept in its “closed” form by the covering of the effector domain CARDs with the helicase domain, hence it is inactivate. Upon viral infection, RIG-I directly binds to viral RNA released into the cytoplasm via the helicase domain and CTD, and then undergoes an ATP-dependent conformational change to take its “open” form (Figure 1-2). Activated RIG-I exposes the CARDs which TRIM25 then modifies with covalent K63-polyubiquitin linkage, and then it forms filamentous oligomerization along with viral RNA [4-6]. Subsequently, RIG-I associates with a downstream CARD-containing adaptor protein termed IFN-β promoter stimulator-1 (IPS-1) (also known as MAVS, VISA, or Cardif), which is anchored to the mitochondrial outer membrane [7-10]. Upon association, IPS-1 forms a prion-like aggregation on the membrane [11] driven by the optimal regulation of mitochondrial

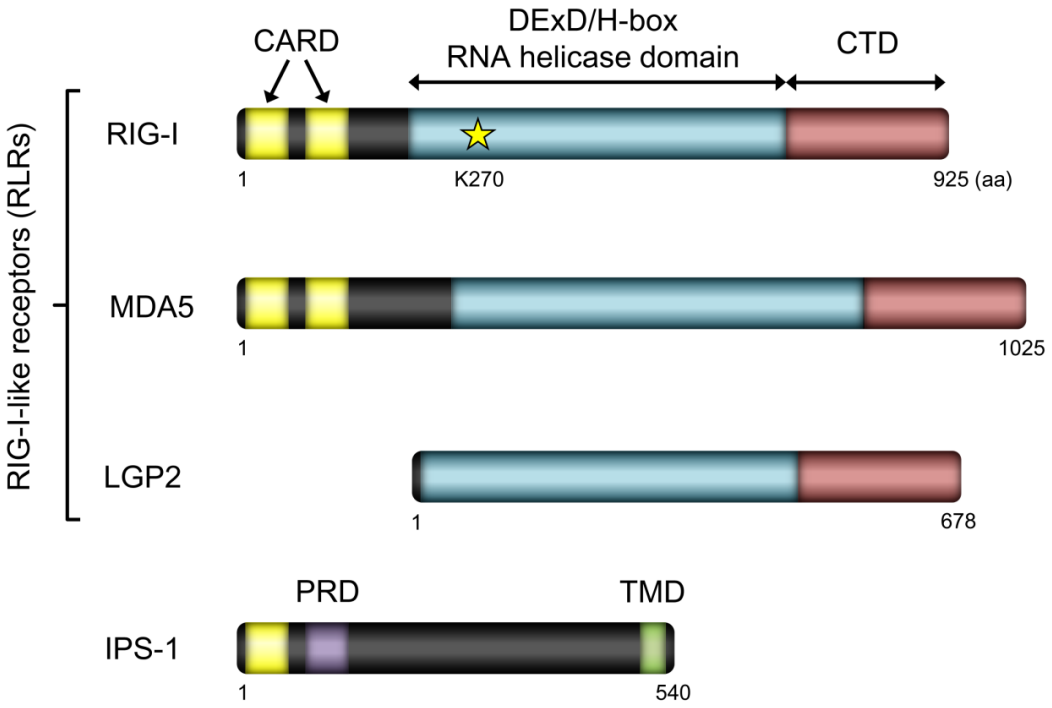

Figure 1-1. Domain structure of RLRs and IPS-1

RIG-I and MDA5 consist of N-terminal tandem CARDs, intermediate DExD/H-box RNA helicase domain, and C-terminal domain (CTD). LGP2 lacks the CARDs. A critical residue for the ATP binding activity of RIG-I is shown by the yellow star (K270). IPS-1 consists of an N-terminal single CARD, proline-rich domain (PRD), and C-terminal transmembrane domain (TMD). IPS-1 is anchored to the mitochondrial outer membrane via TMD.

fusion and fission by MFN1 and OPA1 [12]. The CARD-CARD interaction of RIG-I with IPS-1 serves as a scaffold for the assembly of a protein complex consisting of TRAF3/6 [9, 13], caspase-8/10 [14], RIP1 [7], and TRADD [15]. Formation of the complex further recruits kinase complexes, such as TBK1/IKK-I [16, 17] and IKKα/IKKβ/IKKγ [18-22] leading to activation of transcription factors, IRF-3/7 and NF-κB. These transcription factors in turn translocate into the nucleus and activate the genes coding for Type I and III IFNs (IFN-α/β and IFN-λ) [23] and a set of

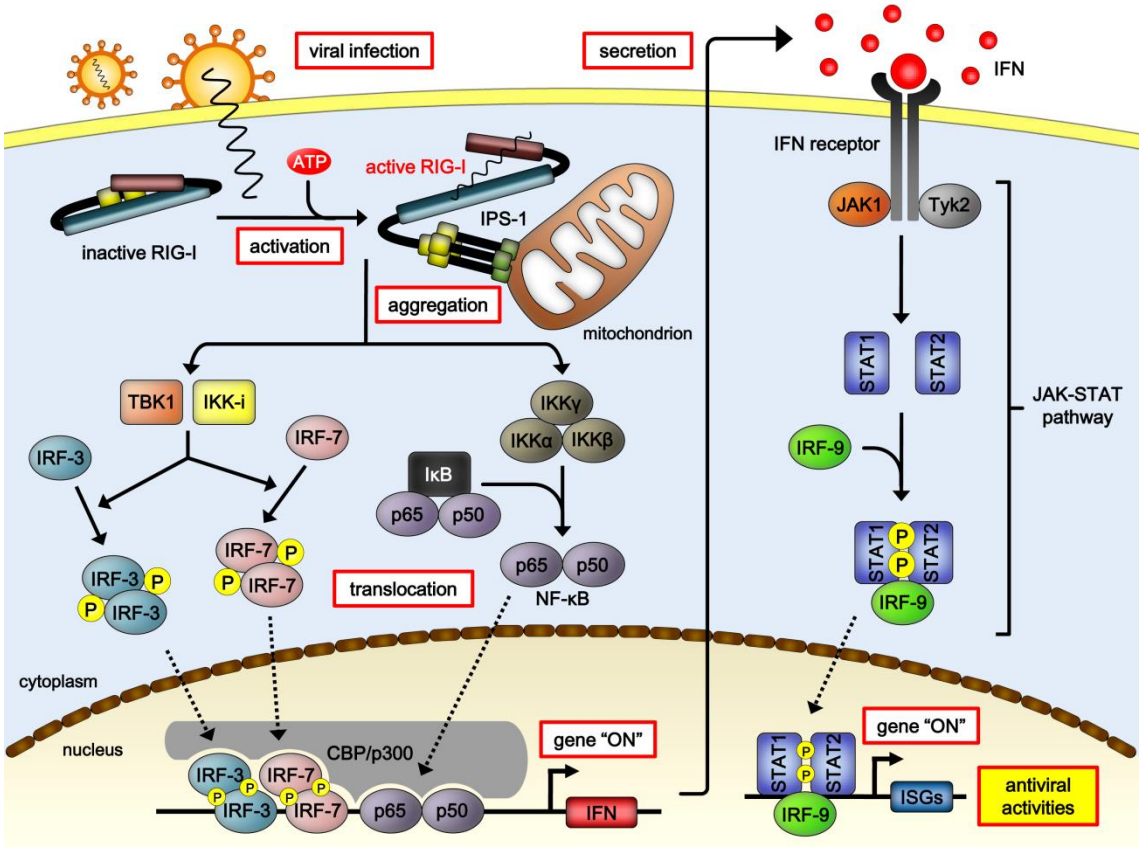

Figure 1-2. RIG-I-driven IFN signaling pathway

Upon viral infection, RIG-I binds to viral RNA via the helicase domain and CTD, and undergoes ATP-dependent conformational change to take active form. Exposed RIG-I CARDs are oligomerized and then interact with the CARD of adaptor protein, IPS-1 that aggregates on the mitochondrial outer membrane. Consequently, a set of kinases such as TBK-1/IKK-i and IKKα/IKKβ/IKKγ are recruited and activate transcription factors, IRF-3/7 and p65/p50 (NF-κB). These transcription factors translocate to the nucleus and activate gene transcription for IFNs cooperating with CBP/p300. Produced IFNs are secreted from the cells, and bind to IFN receptors expressed on the surface of neighboring cells. Finally, the JAK-STAT signaling pathway is activated and hundreds of ISGs are expressed for antiviral activities.

proinflammatory cytokines in collaboration with co-activator, CBP/p300 [24]. Produced IFNs are secreted from the infected cells and binds to cognate receptors expressed on both IFN-producing cells and neighboring cells. Eventually, the JAK-STAT signaling pathway is activated to induce the expression of hundreds of IFN-stimulated genes (ISGs), which encode a variety of antiviral proteins. These proteins also include signaling molecules such as RIG-I and IRF-7, thereby IFN production is positively amplified for intense antiviral activity.

1-2-3. Detection

Among RLRs, RIG-I and MDA5 share extremely similar domain structures and signaling pathways, however, their recognitions are quite different; suggesting a non-redundant role of RLRs in viral detection (Table 1-1). RIG-I detects a wide variety of RNA viruses such as Sendai virus (SeV), Newcastle disease virus (NDV), respiratory syncytial virus (RSV), vesicular stomatitis virus (VSV), influenza A virus (IAV), and hepatitis C virus (HCV), which all belong to negative-sense ssRNA (ssRNA(-)) virus families [25-28]. On the other hand, MDA5 exclusively recognizes viruses belonging to a positive-sense ssRNA virus family, *Picornaviridae*, such as encephalomyocarditis virus (EMCV), Mengo virus, coxackie virus, and enterovirus [29-31]. Vaccinia virus (VACV), a DNA virus belonging to *Poxviridae*, is recognized by MDA5 [32, 33]; however, the myxoma virus of this family is recognized by RIG-I [34]. Moreover, both RIG-I and MDA5 are often required for the recognition and sufficient antiviral response against certain types of viruses such as Semliki Forest virus [35], measles virus [36], West Nile virus [37, 38], dengue virus [37], and reovirus [37, 39]. It is quite possible

that these differential roles in the recognition of viral infections are due to the distinct structures of viral genomes. LGP2, on the other hand, lacks the CARDs unlike RIG-I and MDA5. Therefore, LGP2 was assumed to play a more negative role in the IFN system; however, its positive regulatory activity in antiviral response against certain viruses (*e.g.* NDV, VSV, and EMCV) has been reported [40].

1-2-4. Ligands

The properties of RNA ligands for RIG-I and MDA5 have been extensively explored by means of artificially synthesized RNAs (Table 1-2). Both RIG-I and MDA5 have been shown to be activated by a synthetic dsRNA, poly(I:C), and induce a strong IFN response [3, 39]. Nonetheless, relatively short poly(I:C) (<300 bp) was preferentially recognized by RIG-I whereas long poly(I:C) (>4 kbp) was an exclusive substrate of MDA5; suggesting that the length of dsRNA is an important determinant of the ligand specificity of RIG-I and MDA5 [39].

Along with dsRNA, *in vitro*-transcribed ssRNA by phage RNA polymerase, such as T7-Pol, was also reported to be a good inducer of IFN. *In vitro* transcripts contain a 5'-triphosphate, and this signature appeared to be a critical determinant of non-self recognition by RIG-I [41]. This seems to be a rational strategy to discriminate between non-self and self RNA because the 5'-triphosphate moiety of the host RNA is removed or masked by the RNA processing. Viruses belonging to *Picornaviridae* evade RIG-I detection because their 5'-triphosphate is masked by covalently attached viral protein, Vpg [42, 43]. The *in vitro* transcripts, in addition, present short base-paired structure (*i.e.* double-stranded) at the terminus by the "copy-back" mechanism. This structure was

also demonstrated to be a potent enhancer of the stimulatory 5’-triphosphate ssRNA [44, 45]. Indeed, the genome of IAV contains 5’-triphosphate and partial double-stranded structure (>15 bp) termed the “panhandle”, thereby being a natural ligand of RIG-I [28]. Likewise, SeV generates defective-interfering (DI) viral genomes with a hairpin-like double-stranded structure (100-1,000 bp), and this “snap-back” structure likely represents a ligand of RIG-I [46]. Of note, not only viral genomes but also replicative intermediate RNAs are capable of presenting a dsRNA structure. A variety of ssRNA viruses, which are partially recognized by RIG-I, have been reported to produce substantial amounts of cytosolic viral dsRNA during their life-cycle [47, 48]. Recently, it was shown that RIG-I also recognize base-paired 5’-diphosphate RNA species, and this recognition is essential for responding to reovirus infection [49]. In addition to the structural specificity, sequence dependency of RIG-I recognition has been reported. Activation of RIG-I in response to HCV infection required poly(U/UC) tract at its 3’-UTR along with 5’-triphosphate [27]. Furthermore, the AU-rich sequence in IAV 3’-UTR was recognized by RIG-I, however, 5’-triphosphate moiety was dispensable [50]. Multiple determinants of the non-self RNA recognition of RIG-I are being considered.

Concerning MDA5 ligands, genomes of EMCV and VACV form high molecular weight complex interlaced with ssRNA and dsRNA [32]; and this “RNA web” structure was considered to be involved in MDA5 activation. However, neither the precise structure of the complex nor its recognition mechanism by MDA5 is still enigmatic.

Table 1-1. Viruses recognized by RIG-I and MDA5

RLRs	Viruses	Families; Genome types	References
RIG-I	Sendai virus Newcastle disease virus Respiratory syncytial virus	*Paramyxoviridae*; ssRNA(-), non-segmented	Yoneyama, Kato *et al.* (2005) Kato *et al*. (2005) Loo *et al*. (2008)
	Rabies virus vesicular stomatitis virus	*Rhabdoviridae*; ssRNA(-), non-segmented	Hornung *et al*., 2006 Yoneyama, Kato *et al*. (2005)
	Rift Valley fever virus La Crosse virus	*Bunyaviridae*; ssRNA(-), non-segmented	Weber *et al.* (2013) Weber *et al.* (2013)
	influenza A virus influenza B virus	*Orthomyxoviridae*; ssRNA(-), segmented	Kato *et al*. (2006) Loo *et al*. (2008)
	hepatitis C virus Japanese encephalitis virus	*Flaviviridae*; ssRNA(+), non-segmented	Saito *et al*. (2007) Kato *et al*. (2006)
	Epstein-Barr virus	*Herpesviridae*; dsDNA	Samanta *et al*. (2008)
	myxoma virus	*Poxviridae*; dsDNA	Wang *et al*. (2008)
MDA5	encephalomyocarditis virus Mengo virus coxackie virus enterovirus	*Picornaviridae*; ssRNA(+), non-segmented	Kato, Gitlin *et al*. (2006) Kato *et al*. (2006) Kato *et al*. (2006) Feng *et al*. (2012)
	vaccinia virus	*Poxviridae*; dsDNA	Pichlmair, Delaloye *et al*. (2009)
RIG-I + MDA5	measles virus	*Paramyxoviridae*; ssRNA(-), non-segmented	Ikegame et al. (2010)
	Semliki Forest virus	*Togaviridae*; ssRNA(-), non-segmented	Schulz et al. (2010)
	West Nile virus Dengue virus	*Flaviviridae*; ssRNA(+), non-segmented	Loo *et al*. (2008) Loo *et al*. (2008)
	Reovirus	*Reoviridae*; dsRNA	Kato, Loo *et al*. (2008)

ssRNA: single-stranded RNA, dsRNA: double-stranded RNA, dsDNA: double-stranded DNA, (-): negative-sense genome, (+): positive-sense genome

Table 1-2. Structures of RIG-I and MDA5 ligands

RNA types	Structures	RLRs	References
short Poly(I:C) dsRNA >300 bp	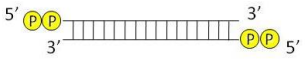	RIG-I	Kato *et al*. (2008)
long Poly(I:C) dsRNA >4 kbp	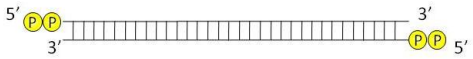	MDA5	Kato *et al*. (2008)
in vitro T7 transcript ssRNA (copy-back)		RIG-I	Schlee *et al*. (2009) Schmidt *et al*. (2009)
IAV genome ssRNA (panhandle)	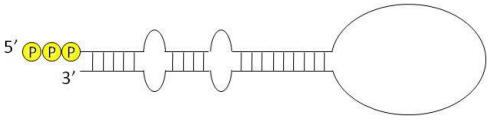	RIG-I	Rehwinkel *et al*.(2010)
SeV genome ssRNA (DI, snap-back)	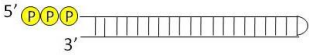	RIG-I	Strähle *et al*. (2007)
HCV genome ssRNA (homopolymer)		RIG-I	Saito *et al*. (2008)
EMCV genome ss/dsRNA (RNA web)	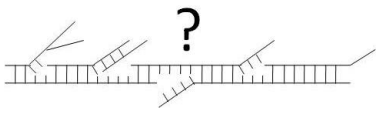	MDA5	Pichlmair *et al*. (2009)

ssRNA: single-stranded RNA, dsRNA: double-stranded RNA

1-3. Stress granules

Cells face a lifetime risk of being exposed to external stresses from their environment. Consequently, cells connaturally equip intrinsic anti-stress strategies to survive from such unfavorable circumstances. These stresses include, for instance, UV exposure, heat shock, oxidation, ER stress, and starvation. Viral infection is also a pivotal stressor that stimulates cells to execute an anti-stress response. Upon these stress signals, four protein kinases, HRI, PERK, GCN2, and dsRNA-inducible protein kinase R (PKR) are activated to phosphorylate an α-subunit of eIF2 (eIF2α) (Figure 1-3). Subsequently, cells provisionally interrupt the translational machinery in order to avoid excrescent protein synthesis and shelter accumulated mRNA by sequestering them in cytoplasmic RNA-protein (RNP) complexes, termed stress granules (SGs) [51]. A SG is typically composed of 40S ribosomal subunits, a subset of translation initiation factors (eIF2, 2B, 3, 4A, 4B, 4E and 4G), and host RNA-binding proteins such as Ras GTPase-activating protein-binding protein (G3BP), poly(A)-binding protein (PABP), human antigen R (HuR), T-cell intracellular antigen-1 (TIA-1), and its related protein TIAR [51-55].

A variety of viruses have been shown to induce the formation of SGs in infected cells [56]. SG formation is strictly regulated in a steady state, however, once cells are exposed to viral infections, PKR is activated by viral dsRNA (vdsRNA) generated as an intermediate product within the viral replicative life-cycle [57]. Recently, SG was reported to play a positive role in antiviral IFN signaling against IAV lacking an IFN-inhibitory NS1 protein (IAVΔNS1) by recruiting RIG-I and a set of antiviral host proteins to detect the viral infection [58]. Moreover, another DExD/H-box RNA

helicase protein DHX36 acts with PKR to induce SGs, thereby facilitates detection of viral RNA by RIG-I [59]. These findings shed light on the function of SGs as antiviral SGs (avSGs), a substantial platform for IFN-inducing signaling triggered by RIG-I.

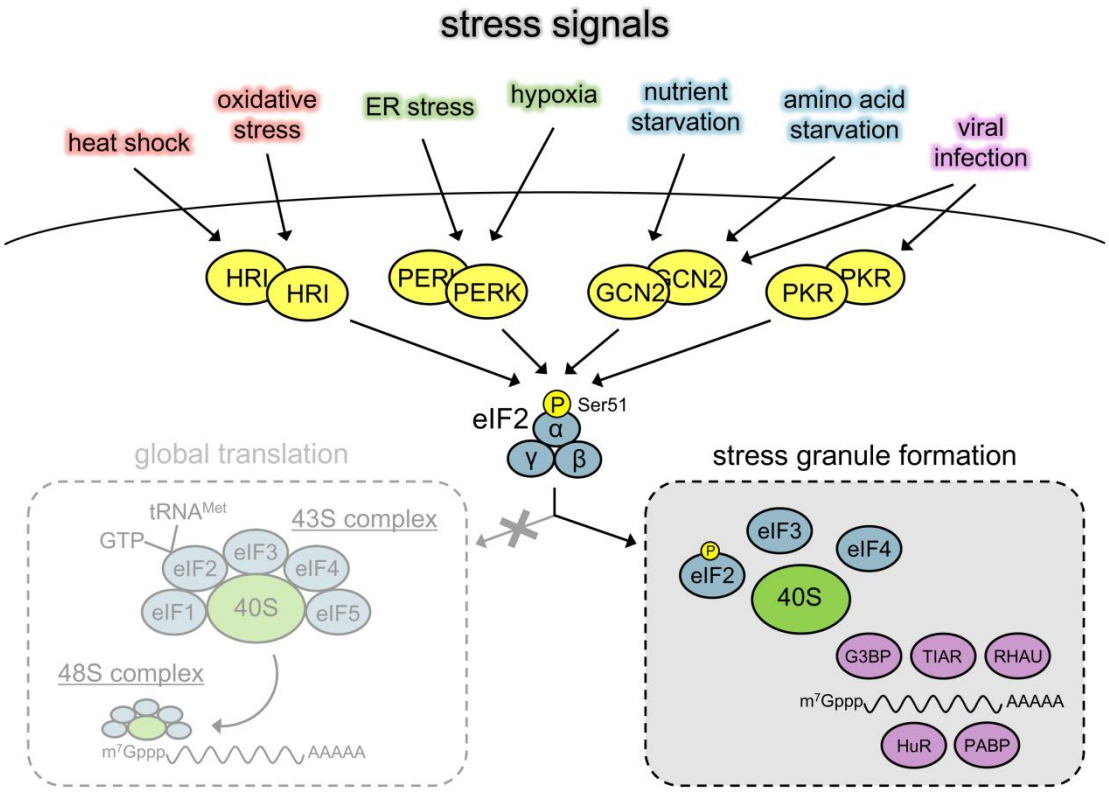

Figure 1-3. Stress granule formation

Protein kinases such as HRI, PERK, GCN2, or PKR are respectively activated depending on the type of stress signals. These kinases are dimerized and undergo autophosphorylation. Activated kinases then phosphorylate α-subunit of eIF2 (eIF2α) and this leads to the dissociation of the eIF2-GTP-tRNA^{Met} complex and the termination of functional translation machinery. Untranslated mRNAs are then sequestered into stress granule composed of RNA-binding proteins.

1-4. ssRNA(-) viruses: structure and replication

ssRNA(-) viruses, which belong to Group V on the Baltimore classification, utilize negative-sense ssRNA as their genetic materials. The ssRNA viruses are classified into positive or negative according to the sense or polarity of their genomes. A negative genome is further distinguished by means of its segmentation as non-segmented and segmented. Since the negative sense viral genomic RNA (vgRNA) is complementary to the positive sense viral messenger RNA (vmRNA), it must be transcribed into the positive sense by RNA polymerase before translation.

Order *Mononegavirales*, a major subgroup of ssRNA(-) viruses, consists of four families; *Bornaviridae*, *Filoviridae*, *Paramyxoviridae*, and *Rhabdoviridae*. Viruses belonging to this order share an extremely similar genetic structure, and their genes typically encodes a nucleocapsid protein (N), phosphoprotein (P), matrix protein (M), fusion protein (F), hemagglutinin-neuraminidase protein (HN), and large RNA-dependent RNA polymerase protein (RdRp/L). These genes are arranged on non-segmented vgRNA with an extracistronic sequence, known as leader (Le) and trailer (Tr), in an order corresponding to 3'-Le-N-P-M-F-HN-L-Tr-5' [60] (Figure 1-4). The viral RdRp first transcribes the Le sequence into positive-sense RNA without terminal modification [61]. After Le transcription, the RdRp re-initiates transcription for the N gene to yield N mRNA with a 5'-m^7G cap and 3'-poly(A) tail. Similarly, the polymerase synthesizes other vmRNA by transcribing downstream genes without dissociation from the template. In later stages of the infection, polymerase switches to replication mode in order to synthesize the entire length of antigenomic RNA (viral complementary RNA (vcRNA)) as a template for synthesis of vgRNA. The general

strategies of transcription and replication are similar across ssRNA(-) viruses [62] (Figure 1-5), and the viral RNA species produced during the replication cycle are sensed by RLRs [28, 29, 37].

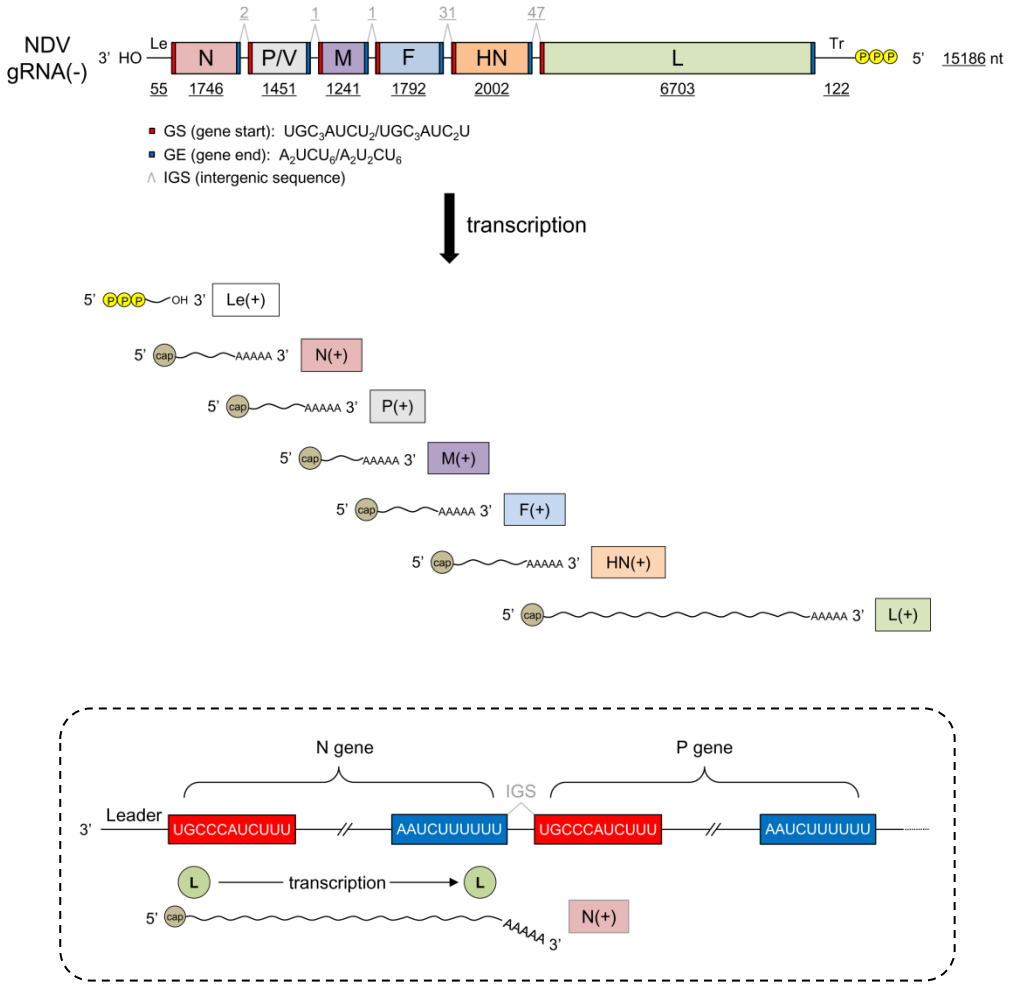

Figure 1-4. Transcription of NDV gRNA

A model for transcription of a typical *Mononegavirales* virus, NDV, is shown. NDV genes are arranged on negative-sense gRNA in the order 3'-Le-P-M-F-HN-L-Tr-5' with the intermediate IGS. The length of each sequence is indicated (nt; nucleotide). Viral RdRp (L) first transcribes Le sequence into short positive-sense transcripts (Le(+)). After this, RdRp starts transcription of the N gene from its GS region and terminates at the GE region (highlighted beneath). RdRp re-initiates the next P gene transcription in the same manner, and continues this toward the last L gene. Transcripts are all 5'-capped and 3'-polyadenylated by RdRp, except for Le(+).

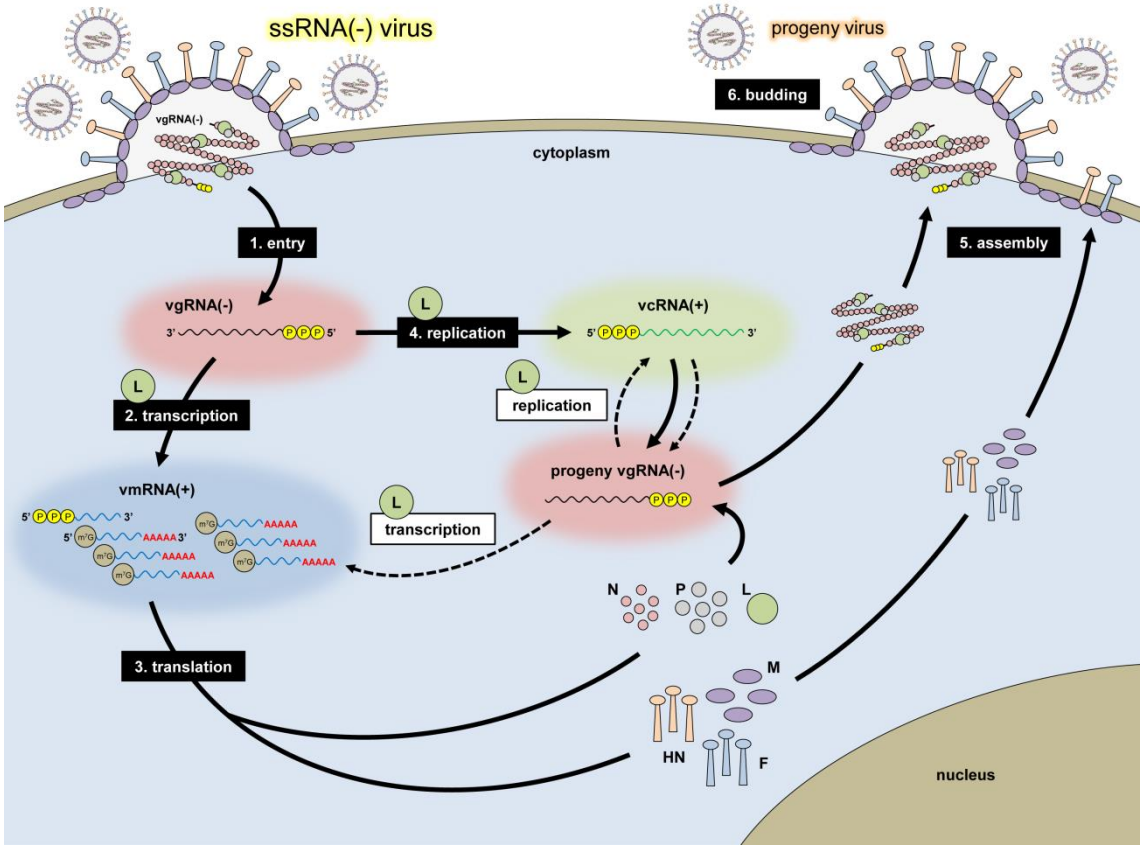

Figure 1-5. Life-cycle of ssRNA(-) viruses

After entry (*step 1*), vgRNA(-) is transcribed by RdRp (L) to produce vmRNA(+) (*step 2*) and viral proteins are synthesized (*step 3*). After an adequate amount of proteins are produced, RdRp switches to RNA replication via the synthesis of antigenomic vcRNA(+) (*step 4*). Replication produces more vgRNA(-) for further transcription (white box) and translation of vRNAs, and for assembly with the structural proteins; N, P, and L (*step 5*), to produce progeny virus particles (*step 6*).

1-5. Aim of this study

In the past decade or so, since RIG-I was first identified as a critical PRR for viral RNA sensing, multitudes of studies have been carried out to explore its ultimate RNA ligands and adversarial viruses. By grace of those challenges, we are now well-informed about a unique architecture of the ligands within a wide variety of viruses which activate RIG-I, and a broad composition of antiviral IFN signaling which RIG-I drives. Nonetheless, in the context of authentic viral infection, how RIG-I spatially and temporally encounters viruses to commence its signaling has not been fully described thus far. In this study, I investigated the spatiotemporal action of RIG-I, especially in line with the dynamics of viral replication, to understand a more fundamental role of RIG-I in the viral RNA sensing and antiviral IFN system.

2. Materials and Methods

2-1. Cells

HeLa (#CCL-2.2, ATCC), FLAG-RIG-I/HeLa (derived from HeLa; #CCL-2.2, ATCC), FLAG-IPS-1/HeLa (derived from HeLa; #CCL-2.2, ATCC) [12], EGFP-G3BP1/HeLa (derived from HeLa; #CCL-2.2, ATCC) [63], HEp-2 (#CCL-23, ATCC), BHK21 (#CCL-10, ATCC) cells, and MEFs (isolated from embryos under C57BL/6 background, Japan SLC, Inc.) were maintained in Dulbecco's Modified Eagle's Medium (DMEM) (Nacalai Tesque) supplemented with 10% Fetal Bovine Serum (FBS) (BioWest) and 1% Penicillin-Streptomycin Mixed Solution (100 U/ml and 100 μg/ml respectively) (Nacalai Tesque).

2-2. Viruses and infection

NDV (strain Miyadera/51) was inoculated into 9-day embryonated chicken eggs and incubated for 2 days at 37°C, followed by overnight incubation at 4°C. Allantoic fluid containing NDV was collected from dead eggs. RSV (strain Long, ATCC VR-26) and VSV (strain Indiana, M mutant) were propagated in HEp-2 cells and BHK21 cells respectively, and culture supernatant was collected. The virus titer was determined by a plaque assay using HEp-2 cells. Virus was added to cells at a multiplicity of infection (MOI) of 1. After 1-hour incubation, the medium was replaced with fresh DMEM and incubated for the indicated hours of infection.

2-3. Arsenite, nocodazole, and RNase treatments

Sodium arsenite, nocodazole, and ribonuclease (RNase) A were purchased from SIGMA-ALDRICH. ShortCut RNase III was purchased from New England Biolabs. Cells were treated as described in the figure legends.

2-4. Immunofluorescence

Cells were fixed with 4% paraformaldehyde solution for 10 minutes at room temperature. A 0.5% Triton X-100 solution was added to the cells for permeabilization and incubated for 5 minutes at room temperate. Regarding blocking, 0.5 mg/ml BSA solution in PBST (PBS containing 0.04% Tween-20) was added to the cells and incubated for 30 minutes at room temperature. Primary antibodies were diluted in 0.5 mg/ml BSA/PBST and added to the cells, then incubated overnight at 4°C. After washing with PBST, secondary antibodies were added to the cells at a 1:1,000 dilution in 0.5 mg/ml BSA/PBST, and incubated for 1 hour at room temperature. After washing with PBST, 1 μg/ml DAPI solution in PBS was added to the cells to stain the nucleus. Cells were briefly rinsed with PBS, and then mounted with Fluromount-G (SouthernBiotech). Images were taken by the confocal laser scanning microscope, TCS-SP8 (Leica Microsystems). The primary antibodies used were; anti-NDV-N mouse mAb (provided by Dr. T. Sakaguchi, Hiroshima University in Japan), anti-TIA-1 goat pAb (#sc-1751, Santa Cruz Biotechnology), anti-TIAR rabbit mAb (#8509, Cell Signaling Technology), anti-TIAR goat pAb (#sc-1749, Santa Cruz Biotechnology), anti-G3BP1 mouse mAb (#sc-365338, Santa Cruz Biotechnology), anti-eIF3η

(#sc-16377, Santa Cruz Biotechnology), anti-FLAG M2 mouse mAb (#F1804, SIGMA-ALDRICH), and anti-dsRNA/J2 mouse mAb (English & Scientific Consulting Kft.). Anti-IPS-1 guinea pig pAb was provided by Dr. I. Julkunen. Anti-RIG-I and anti-NDV-L antibodies were originally generated by immunizing rabbits with synthetic peptides corresponding to amino acids 793-807 of human RIG-I and 1160-1183 of NDV-L, respectively. The secondary antibodies used were; Alexa Fluor 488 donkey anti-rabbit IgG H+L (#A-21206), Alexa Fluor 488 donkey anti-mouse IgG H+L (#A-21202), Alexa Fluor 488 Donkey anti-Goat IgG H+L (#A-11055), Alexa Fluor 594 Donkey anti-Rabbit IgG H+L (#A-21207), Alexa Fluor 594 Donkey anti-Mouse IgG H+L (#A-21203), Alexa Fluor 633 Goat anti-Mouse IgG H+L (#A-21050), Alexa Fluor 633 Donkey anti-Goat IgG H+L (#A-21082), and Alexa Fluor 647 Donkey anti-Goat IgG H+L (#A-21447), all purchased from Life Technologies.

2-5. RNA-FISH

RNA-FISH assay was performed using the QuantiGene ViewRNA ISH Cell Assay Kit (Affymetrix) according to manufacturer's instructions as below. Cells were fixed in 4% paraformaldehyde solution for 30 minutes and permeabilized for 5 minutes with detergent solution. Protease solution was added to the cells at a 1:4,000 dilution in PBS and incubated for 10 minutes. After washing with PBS, the cells were incubated with a probe set at a 1:25 dilution for 3 hours at 40°C. The cells were further and independently incubated with a pre-amplifier, amplifier, and label probe (all at a 1:25 dilution) for 30 minutes at 40°C. After washing with PBS, the cells were subjected to an immunofluorescence assay. The probe sets used were; *NDV-F*(-) (#VF1-15407),

NDV-N(+) (#VF4-15408), and human *IFNB1* (#VA1-11281), all purchased from Affymetrix.

2-6. Computer-based statistical cell analysis

Confocal micrographs of NDV-infected or arsenite-treated cells were subjected to the automatic analysis module (Multi Wavelength Cell Scoring) of MetaMorph Software v7.7 (Molecular Devices) in order to count vRC and SG speckles and *IFNB* mRNA dots. Briefly, the total cell number was first determined by counting the number of nuclei in the DAPI channel. A single cell area was segmented from the TIAR or eIF3η channel in reference to the intercellular boundary of the cytoplasmic staining area. The numbers of vRC (N), SG (TIAR or eIF3η), and *IFNB* mRNA were counted from each channel.

2-7. RNAi gene knockdown

siRNAs for *RIG-I/DDX58* (HSS119008), *PKR* (HSS108571), *G3BP1* (HSS115444), *G3BP2* (HSS114988), and a negative control (#12935-300), purchased form Life Technologies, were transfected into 1×10^5 HeLa cells at a final concentration of 10 nM using Lipofectamine RNAiMAX Reagents (Life technologies). 24 hours after transfection, the cells were transferred to new culture plates with fresh DMEM. After being incubated for a further 24 hours, cells were subjected to the following experiments.

2-8. Western blotting

Cells were lysed with ice-cold NP-40 lysis buffer (50 mM Tris-HCl [pH 8.0], 150 mM NaCl, 1% NP-40, 1 mM sodium orthovanadate, 1 mM PMSF, and 0.1 mg/ml leupeptin). After centrifugation, the supernatant was collected, mixed with an equal volume of 2× SDS sample buffer (125 mM Tris-HCl [pH 6.8], 4% SDS, 20% glycerol, 0.01% BPB, and 10% 2-mercaptoethanol), and boiled for 5 minutes. The sample corresponding to a protein amount of 30 μg was applied to 5-20% gradient e-PAGEL (ATTO), separated by a standard SDS-PAGE method, and then transferred onto an Immobilon-P PVDF membrane (MILLIPORE). The membrane was incubated in Tris-buffered saline with 0.1% Tween-20 (TBST) containing 5% skimmed milk for 30 minutes at room temperature for blocking. The membrane was incubated with a primary antibody diluted in the blocking buffer overnight at 4°C. After washing with TBST, the membrane was incubated with an AP-conjugated secondary antibody diluted in the blocking buffer for 1 hour at room temperature. After washing with TBST, protein bands were visualized using the BCIP-NBT Solution Kit for Alkaline Phosphate Stain (Nacalai Tesque) or ECL Prime Western Blotting Detection Reagent (GE Healthcare). The primary antibodies used were; anti-PKR mouse mAb (#sc-6282, Santa Cruz Biotechnology), anti-phospho-PKR rabbit pAb (#ab13447, Abcam), anti-G3BP2 goat pAb (#sc-161612), anti-STAT1 rabbit pAb (#9172, Cell Signaling Technology), anti-phospho-STAT1rabbit pAb (#9172, Cell Signaling Technology), and anti-β-Actin mouse mAb (#A2228, SIGMA ALDRICH). The secondary antibodies used were; goat anti-rabbit IgG-AP (#sc-2007, Santa Cruz Biotechnology), goat anti-mouse IgG-AP (#sc-2008, Santa Cruz Biotechnology), anti-rabbit IgG, HRP-linked (#7074, Cell

Signaling Technology), and anti-mouse IgG, HRP-linked (#7076, Cell Signaling Technology).

2-9. Reverse transcription and quantitative PCR (RT-qPCR)

Total RNA was isolated from cells using TRIzol Reagent (Ambion), and treated with RNase-Free Recombinant DNase I (Roche Diagnostics). After phenol-chloroform extraction and ethanol precipitation, purified total RNA was subjected to cDNA synthesis using a High-Capacity cDNA Reverse Transcription Kit (Applied Biosystems). Gene expression levels were measured by the StepOnePlus Real-Time PCR system (Applied Biosystems) using the TaqMan Fast Universal PCR Master Mix (Applied Biosystems), and determined by the $2^{-\Delta\Delta Ct}$ relative quantitative method. The TaqMan probes used for measurements were; *IFNB1* (#Hs01077958_s1), *ISG20* (#Hs00158122_m1), *ISG56*/*IFIT1* (#Hs01911452_s1), *CXCL10* (#Hs01124251_g1), *Ifnb1* (#Mm00439552_s1), *Isg56*/*Ifit1* (#Mm00515153_m1), *Cxcl10* (#Mm00445235_m1), and eukaryotic *18S rRNA* (#4333760F), all purchased from Applied Biosystems. The probe for *NDV-N* was designed as below: 5'-GTCCGTATTTGACGAATACGAG-3' (forward primer), 5'-CAAGGGCAACATGGTTCCTC-3' (reverse primer), and 5'-TCAGGCAAGGTGCTC-3' (probe).

2-10. RNA preparation and transfection

Poly(A)$^+$ mRNA was isolated from the total RNA of mock/NDV-infected (12 hpi, MOI = 1) HeLa cells using the Oligotex-dT30 <Super> mRNA Purification Kit

(TaKaRa) according to manufacturer's instructions. Purification was repeated twice to yield a pure poly(A)$^+$ mRNA fraction. The supernatant after centrifugation was subjected to ethanol precipitation in order to obtain a concentrated poly(A)$^-$ RNA fraction. NDV gRNA was isolated from virus particles propagated in the embryonated chicken eggs, as described above. Allantoic fluid was centrifuged overnight at 15,000 rpm at 4°C, and the pellet was lysed using TRIZOL Reagent (Ambion) followed by isopropanol precipitation. 5'-triphosphate RNA was synthesized *in vitro* as reported previously [64]. RNA samples were treated with 1 U of ShortCut RNase III (New England Biolabs), 1 U of RNase-free DNase I recombinant (Roche), and 15 U of Calf Intestine Alkaline Phosphatase (Takara) at 37°C for 30 minutes, or 10 U of Vaccinia Capping Enzyme (New England Biolabs) according to the manufacturer's instruction. After this treatment, RNA samples were purified by phenol-chloroform extraction and ethanol precipitation. Regarding RNA transfection, 200 ng of each RNA sample was transfected into 1×10^5 MEFs or 2×10^5 HeLa cells using Lipofectamine 2000 (Invitrogen) according to the manufacturer's instruction.

2-11. *In vitro* transcription

NDV gRNA isolated from virus particles by TRIZOL Reagent was subjected to reverse transcription, as described above. Synthesized cDNA was further subjected to PCR using primer sets including the T7 RNA polymerase promoter sequence (Table in S1 Table). PCR products were *in vitro* transcribed by the T7 RiboMAX Express Large Scale RNA Production System (Promega) according to manufacturer's instructions. Ribo m^{7}G cap analog (Promega) and Cy3-UTP (GE Healthcare) were included in the

reaction for 5'-m^{7}G capping and Cy3 labeling respectively. Poly(A) Tailing Kit (Ambion) was used for 3'-poly(A) modifications. Unincorporated nucleotides within the samples were removed by NucAway Spin Columns (Ambion). *In vitro* transcribed RNA samples were transfected, as described above.

2-12. Northern blotting

A denaturing agarose gel was prepared at a final concentration of 1% (w/v) Agarose ME (Nacalai Tesque), 1× MESA (Dojindo), 2% formaldehyde (Nacalai Tesque), and 0.5 μg/ml ethidium bromide. A total of 250 ng of each RNA sample was mixed with an equal volume of Gel Loading Buffer II (Ambion) and incubated at 65°C for 15 minutes, followed by quick cooling on ice, and then electrophoresed in 1× MESA. The gel was transferred onto a nylon membrane Hybond-N (GE Healthcare) by a capillary blotting method using 10× SSC Buffer (Nacalai Tesque). After UV cross-linking, the membrane was pre-incubated in PerfectHyb Hybridization Solution (TOYOBO) at 65°C for 20 minutes. An RNA probe was added to the solution and incubated at 65°C overnight. The membrane was washed with 2× SSC (+0.1% SDS) and 0.2× SSC (+0.1% SDS) at 65°C for 15 minutes, and then irradiated onto Storage Phosphor Screen BAS-IP (GE Healthcare). Images were scanned using BAS-5000 Image Analyzer (Fujifilm). In order to prepare RNA probes (N(-) and Le(-)), NDV cDNA was subjected to PCR using primer sets including the T7 RNA polymerase promoter sequence (Table in S1 Table). PCR products were *in vitro* transcribed into [α-^{32}P]-CTP-radiolabeled RNA probes by Riboprobe System-T7 (Promega). Unincorporated nucleotides within the samples were removed by NucAway Spin Columns (Ambion).

2-13. Strand-specific RT-qPCR

Strand-specific RT-qPCR targeting viral RNA was performed as introduced elsewhere [65]. In the RT step, cDNA complementary to the target viral RNA was synthesized with the primer including “5’-tag”, of which sequence is unrelated to NDV, RSV, and VSV (Tables in S2, S3, and S4 Table). After the reaction, RT sample was treated with 10 U of Exonuclease I (New England Biolabs) at 37°C for 1 hour to remove unincorporated primer, and then the reaction was inactivated at 60°C for 30 minutes. The tagged-cDNA was subjected to qPCR analysis with Fast SYBR Green Mater Mix (Thermo Fisher Scientific), using a specific primer set; primer corresponding to tag sequence and viral RNA-specific primer (Tables in S1, S2, and S3 Tables). Standard curve was generated from ten-fold serial dilutions (10^{10}, 10^{9}, 10^{8}, 10^{7}, 10^{6}, 10^{5}, 10^{4}, 10^{3} copies/μl) of vgRNA isolated from viral particles or *in vitro* synthesized viral RNA.

3. Results

3-1. NDV infection induced formation of viral granules and avSGs

To monitor virus infection and avSG formation, I infected HeLa cells with NDV and detected avSG by immunostaining with antibodies to its marker proteins; TIA-1, TIAR, G3BP1, and eIF3η (Figure 3-1). Cytoplasmic granules were not observed in uninfected cells whereas granules containing these avSG markers were clearly detectable at 12 hours post infection (hpi). avSGs were not yet visible at 6 hpi (Figure 3-1A). To correlate avSG formation and viral replication, I monitored the expression of viral proteins; large polymerase (L) and nucleoprotein (N) by immunostaining (Figure 3-2). These viral proteins clearly localized as granules detectable at 6 hpi, when avSGs (shown by TIAR) were undetectable. At 12 hpi, avSGs were detectable as distinct granules from viral granules. Although occasional contact between viral granules and avSGs was observed, no merger neither co-localization was observed.

3-2. NDV viral RNAs were derived from vRCs and vRNA(+) migrated to avSGs

Viral N protein functions as an indispensable component for RNA viruses through association with viral genomic RNA (vgRNA) for its transcription and replication. Viral L protein is a RNA-dependent RNA polymerase that catalyzes viral transcription and replication. Therefore, NDV viral granules containing N and L proteins were likely a locale for viral replication. To address this further, I examined the subcellular localization of NDV viral RNAs by RNA-FISH. At 6 hpi, negative-strand NDV viral

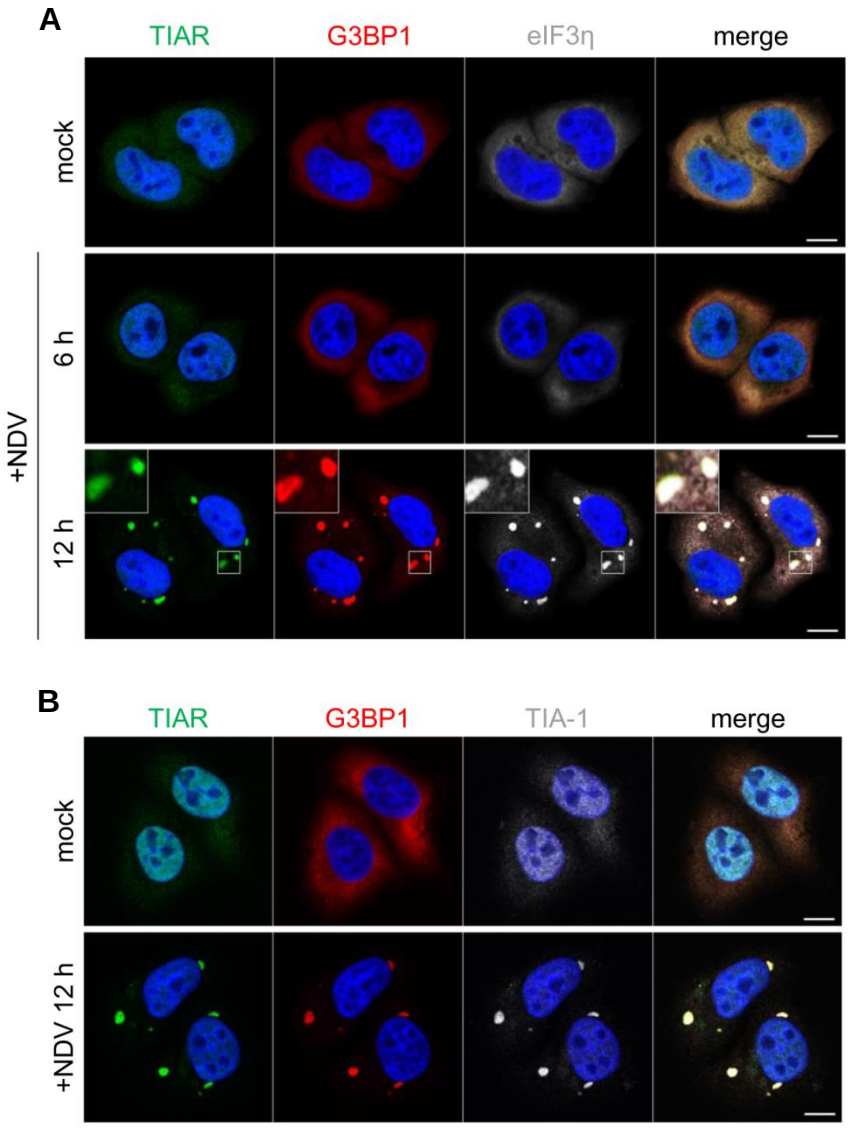

Figure 3-1. NDV infection induced avSGs formation

(A and B) HeLa cells were either mock treated or infected with NDV (MOI = 1) for 6 and 12 hours and then immunostained for TIAR (green), G3BP1 (red), eIF3η (white in A), and TIA-1 (white in B). Nuclei were stained with DAPI (blue). The boxed area of cell image at 12 hpi was enlarged and is displayed in the upper left of the image (A). The white scale bar corresponds to 10 μm.

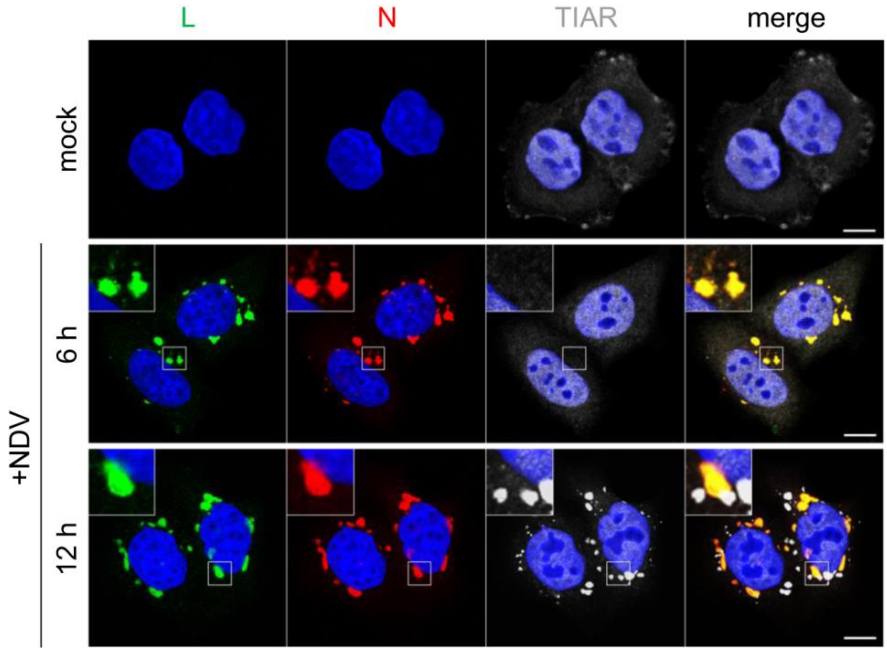

Figure 3-2. NDV infection induced viral granules formation

HeLa cells were either mock treated or infected with NDV (MOI = 1) for 6 and 12 hours. Cells were immunostained for L (green), N (red), and TIAR (white). The boxed area was enlarged and is displayed in the upper left of the image. Nuclei were stained with DAPI (blue). The white scale bar corresponds to 10 μm.

RNA (vRNA(-)) corresponding to vgRNA was detected in viral granules in which N protein localized, and this association persisted at 12 hpi (Figure 3-3A). Based on this observation, I referred to viral granules as viral replication complex (vRC). Positive-strand NDV viral RNA (vRNA(+)), on the other hand, was first detectable as granules co-localized with vRCs at 6 hpi (Figure 3-3A), and interestingly, its localization expanded beyond vRCs to avSGs (shown by TIAR) at 12 hpi (Figure 3-3B). This observation suggested that a portion of vRNA(+) was translocated from vRCs to avSGs by some cue. I observed no detectable background signals in mock-infected cells by RNA-FISH (Figure 3-4).

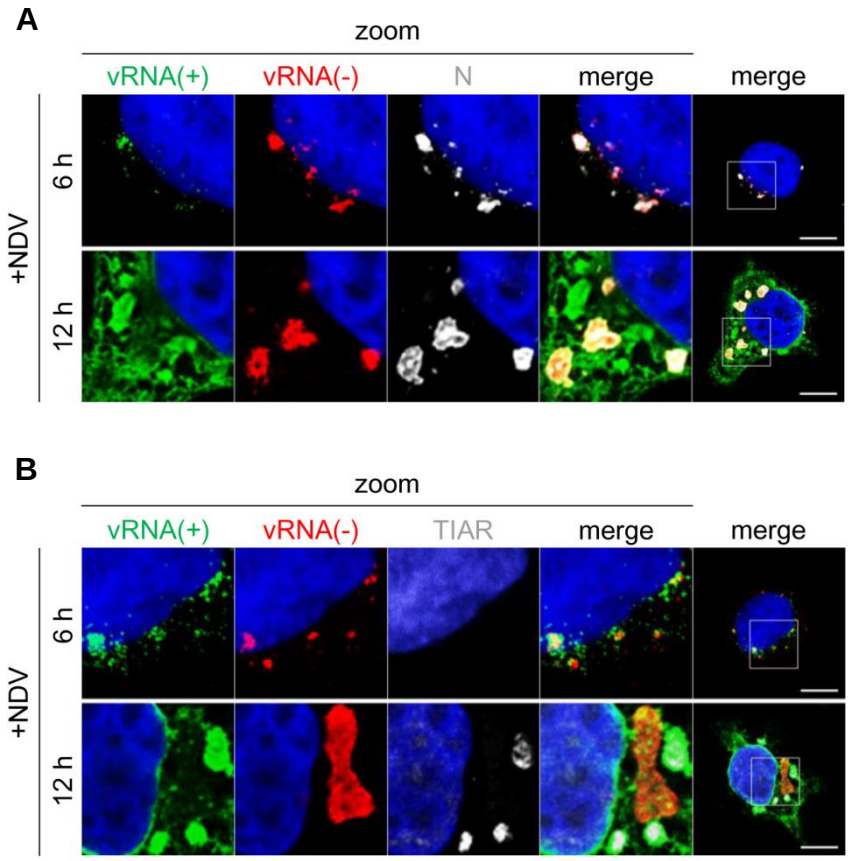

Figure 3-3. Distribution of NDV viral RNAs

(A and B) HeLa cells were infected with NDV (MOI = 1) for 6 and 12 hours, and then NDV vRNA(-) (red) and vRNA(+) (green) were detected by the RNA-FISH method. N (white in A) and TIAR (white in B) were immunostained with their respective antibodies (white). Nuclei were stained with DAPI (blue). A merged image at original magnification is shown in the rightmost panel. The white scale bar corresponds to 10 μm.

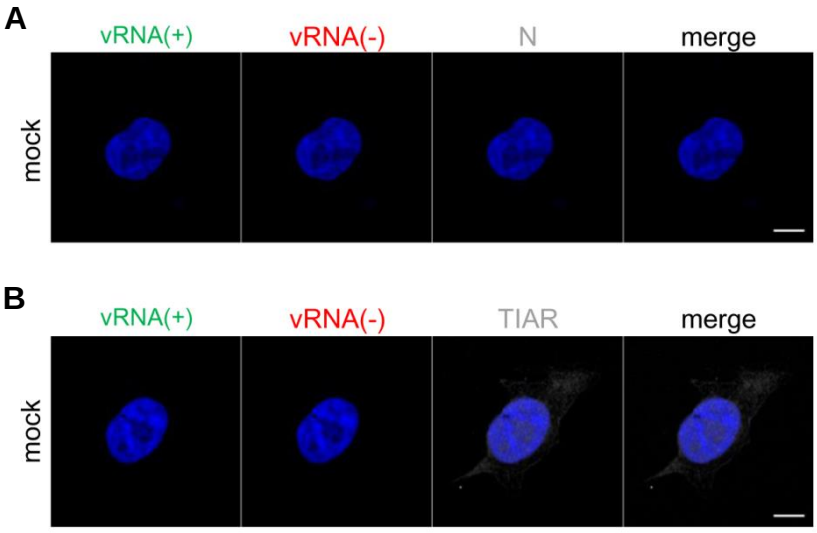

Figure 3-4. Specificity of RNA-FISH

(A and B) Mock-treated HeLa cells were fixed and subjected to RNA-FISH detection for NDV vRNA(+) (green) and vRNA(-) (red). Cells were also immunostained for N (white in A) or TIAR (white in B). Nuclei were co-stained with DAPI (blue). The white scale bar corresponds to 10 μm.

3-3. NDV vdsRNA production was retained in vRCs

It has been reported that certain types of RNA viruses, including NDV, produce viral double-stranded RNA (vdsRNA) as intermediate products within their replicative lifecycle [47, 48]. I further examined localization of NDV vdsRNA by immunostaining with an anti-dsRNA antibody, which detects >40 bp dsRNA (ref). NDV vdsRNA was not detectable at 6 hpi, but was clearly detectable at 12 hpi within vRCs (shown by L) (Figure 3-5A). Interestingly, detection of vdsRNA was restricted to vRCs containing L and vRNA(-), and avSGs containing TIAR and vRNA(+) were apparently devoid of vdsRNA (Figure 3-5B). The antibody specificity was confirmed by loss of the reactivity after ribonuclease digestion (RNase A and III) (Figure 3-6). Taking these observations together, I concluded that NDV exclusively replicated within vRCs, but not within avSGs.

3-4. NDV vRCs formation was synchronized with primary *IFNB* induction

To elucidate the biological significance of vRCs and avSGs in the initiation of antiviral innate immunity, I examined the kinetics of the appearance of these granules along with *IFNB* gene expression. vRCs and avSGs were monitored every 1.5 hours up to 12 hpi by immunostaining (Figure 3-7). vRCs (shown by N) were initially detected at 4.5 hpi as small granules, whose size subsequently increased. avSGs (shown by TIAR) were detectable as late as 7.5 hpi and persisted thereafter. Quantification analysis revealed the temporal appearance of these granules (Figure 3-8A): vRCs-positive cells (light gray) were first detected at 1.5 hpi and reached >90 % at 6 hpi;

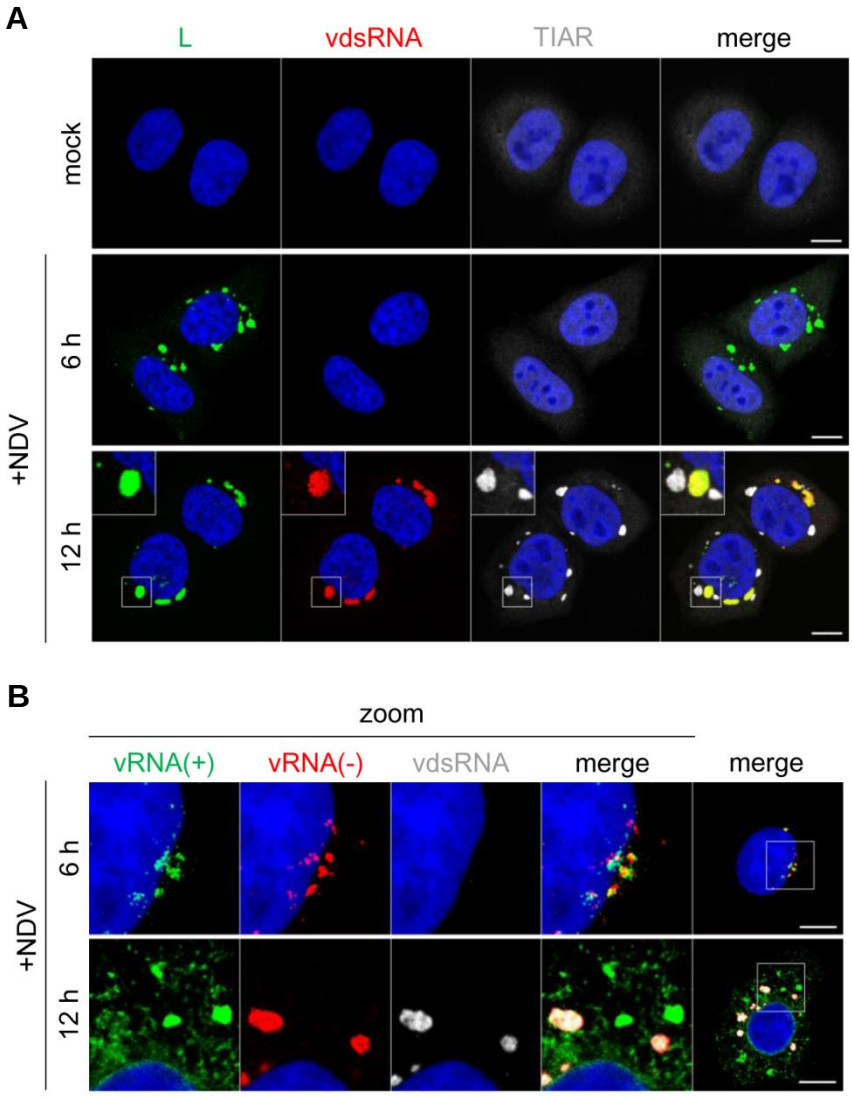

Figure 3-5. Distribution of NDV viral dsRNA

(A and B) HeLa cells were either mock treated or infected with NDV (MOI = 1) for 6 and 12 hours. (A) Cells were immunostained for L (green), vdsRNA (red), and TIAR (white). The boxed area was enlarged and displayed on the upper left of the image. (B) NDV vRNA(-) (red) and vRNA(+) (green) were detected by the RNA-FISH method. NDV vdsRNA was immunostained with a specific antibody (white). A merged image at the original magnification is shown in the rightmost panel. Nuclei were stained with DAPI (blue). The white scale bar corresponds to 10 μm.

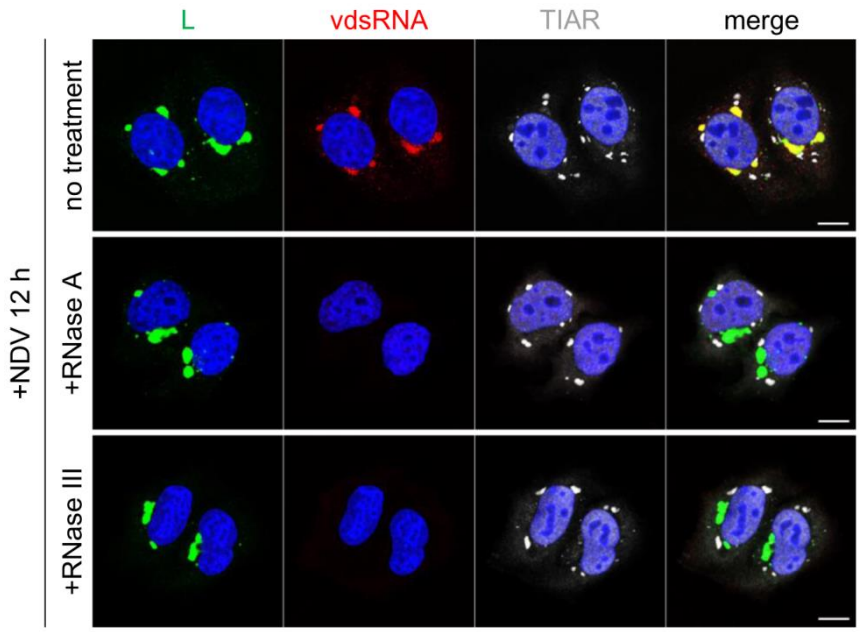

Figure 3-6. Validation for specificity of an anti-dsRNA antibody

HeLa cells infected with NDV for 12 hours (MOI = 1) were fixed and permeabilized, and then treated with 200 μg/ml RNase A (at low NaCl concentration) or 30 units/ml RNase III. The cells were immunostained for L (green), vdsRNA (red), and TIAR (white). Nuclei were stained with DAPI (blue). The white scale bar corresponds to 10 μm.

avSGs-positive cells (black) were detected at 7.5 hpi and reached > 90 % at 12 hpi. It is important to note that cells without vRCs never exhibited avSGs, except for cells treated with arsenite (dark gray), which was used as positive control for SG formation. *IFNB* mRNA accumulation was also visualized by RNA-FISH, and detection correlated well with nuclear translocation of both IRF-3 and NF-κB (Figure 3-9). *IFNB* mRNA was visible from 6 hpi and the number of *IFNB*-positive cells increased thereafter (Figure 3-7). This observation was also shown by quantification analysis (red + green) (Figure 3-8B). At 6 hpi, *IFNB* mRNA-positive cells were all vRCs-positive (red). After 7.5 hpi, cells double-positive for vRCs and avSGs were *IFNB* mRNA-positive (green) and this population increased to 66.1% at 12 hpi, suggesting that this type of cell was the main

producer of IFN-β. Interestingly, cells positive for vRCs and *IFNB* mRNA, but negative for avSGs (red) retained a constant population around 3-5%. A time course of NDV-induced *IFNB* mRNA expression was also monitored by RT-qPCR (Figure 3-8C), confirming that the gene expression was first detected at 6 hpi and markedly increased up to 12 hpi. Since *IFNB* mRNA was detected in cells exhibiting vRCs at 6 hpi (Figure 3-8B), vRC formation is supposed to be responsible for *IFNB* gene expression at 6 hpi, a relatively early phase of infection. In the later phase, however, a population of cells triple-positive for vRCs, avSGs and *IFNB* mRNA (green) dramatically increased, suggesting that avSGs contributed to secondary *IFNB* gene amplification.

3-5. RIG-I accumulated in both NDV vRCs and avSGs

NDV infection is preferentially detected by the cytoplasmic viral RNA sensor, RIG-I, a crucial molecule for IFN induction [29]. Therefore, I further examined the subcellular localization of RIG-I in NDV-infected cells (Figure 3-10). RIG-I co-localized with vRCs (shown by N) at 6 hpi, when avSGs (shown by TIAR) were not yet induced. At 12 hpi, its localization expanded beyond vRCs to avSGs. These results were quite consistent with the observations that formation of vRCs and avSGs coincided with the *IFNB* mRNA accumulation (Figure 3-8B) and nuclear translocation of IRF-3 and NF-κB (Figure 3-10B).

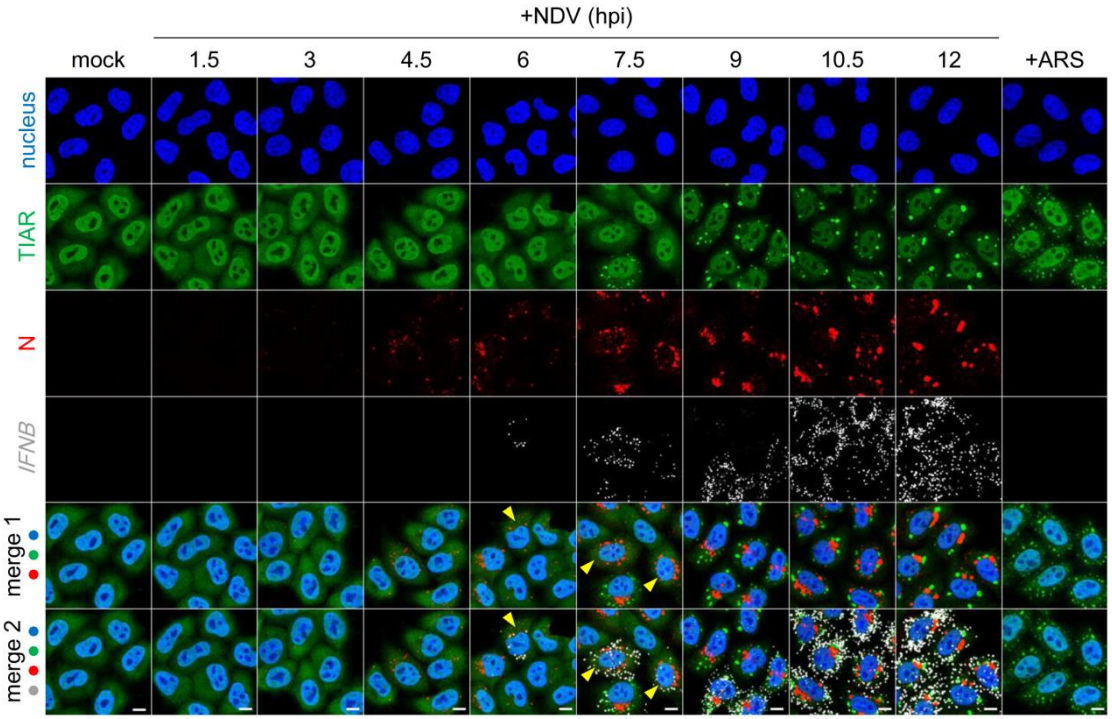

Figure 3-7. Time course of vRCs/avSGs formation and *IFNB* mRNA expression

HeLa cells were infected with NDV (MOI = 1) for the indicated time or treated with 0.5 mM sodium arsenite (ARS) for 30 minutes. After fixation, the cells were immunostained for TIAR (green) and N (red). *IFNB* mRNA (white) was detected by the RNA-FISH method. Nuclei were stained with DAPI (blue). Merge 1: nucleus, TIAR, N, merge 2: nucleus, TIAR, N and *IFNB* mRNA. The yellow arrowheads are cells double-positive for vRC and *IFNB* mRNA (without avSGs). The white scale bar corresponds to 10 μm.

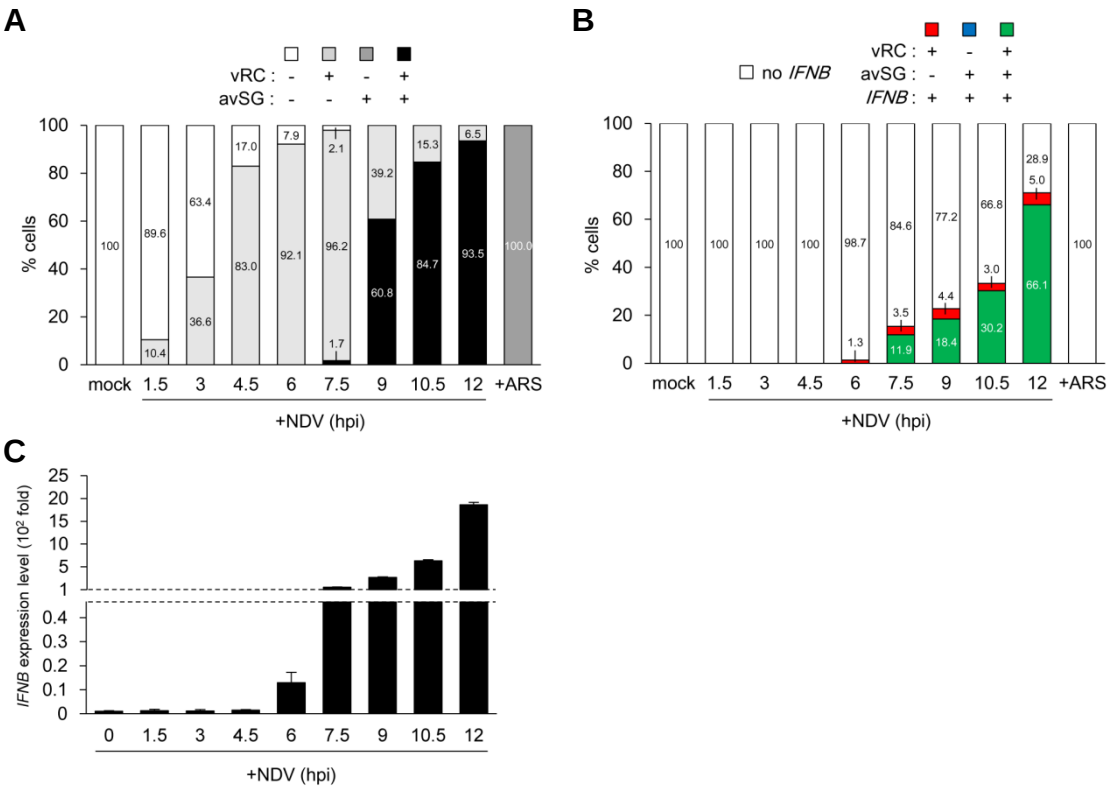

Figure 3-8. Quantification of vRCs/avSGs formation and *IFNB* mRNA expression

(A and B) Approximately 300 HeLa cells at the indicated time points of NDV infection or ARS treatment were counted by MetaMorph software. Cells were categorized according to the existence of vRCs, avSGs, and *IFNB* mRNA as shown above. Percentages are indicated inside the data bar. **(C)** HeLa cells were infected with NDV (MOI = 1) for the indicated time up to 12 hours. Expression levels of *IFNB* mRNA were measured by RT-qPCR. Data is represented as means of ±SD.

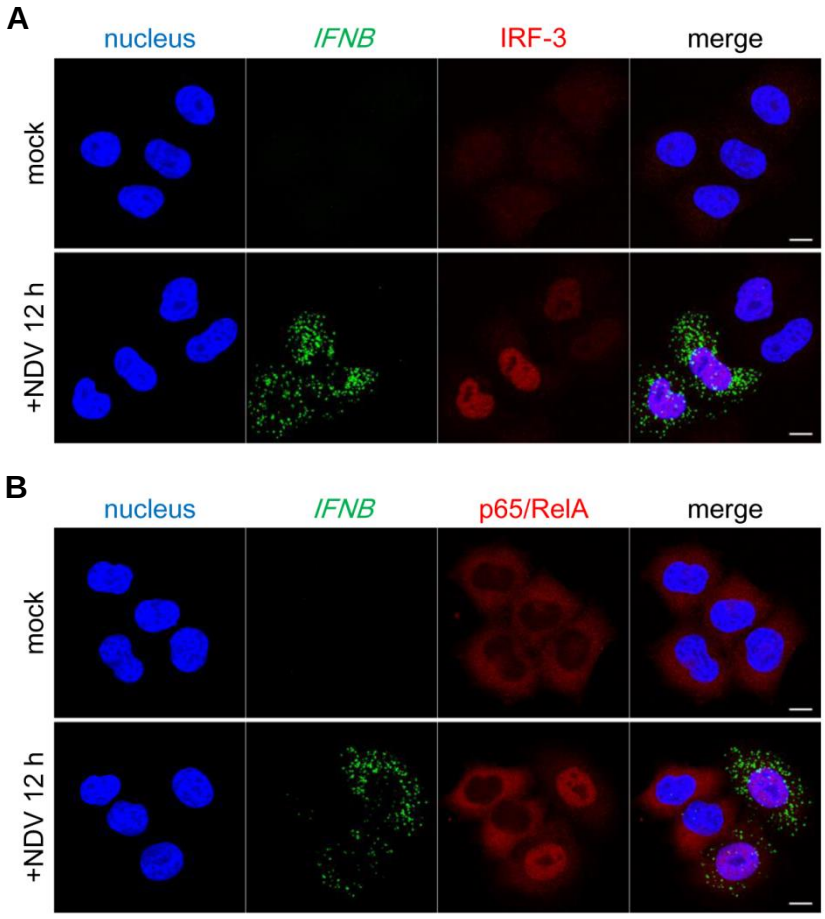

Figure 3-9. Correlation of *IFNB* mRNA FISH and nuclear IRF-3/NF-κB

HeLa cells were either mock infected or infected with NDV (MOI = 1) for 12 hours. *IFNB* mRNA (green) was detected by the RNA-FISH method. IRF-3 (A) and p65/RelA (B) shown in red were immunostained with the respective antibodies. Nuclei were stained with DAPI (blue). The white scale bar corresponds to 10 μm.

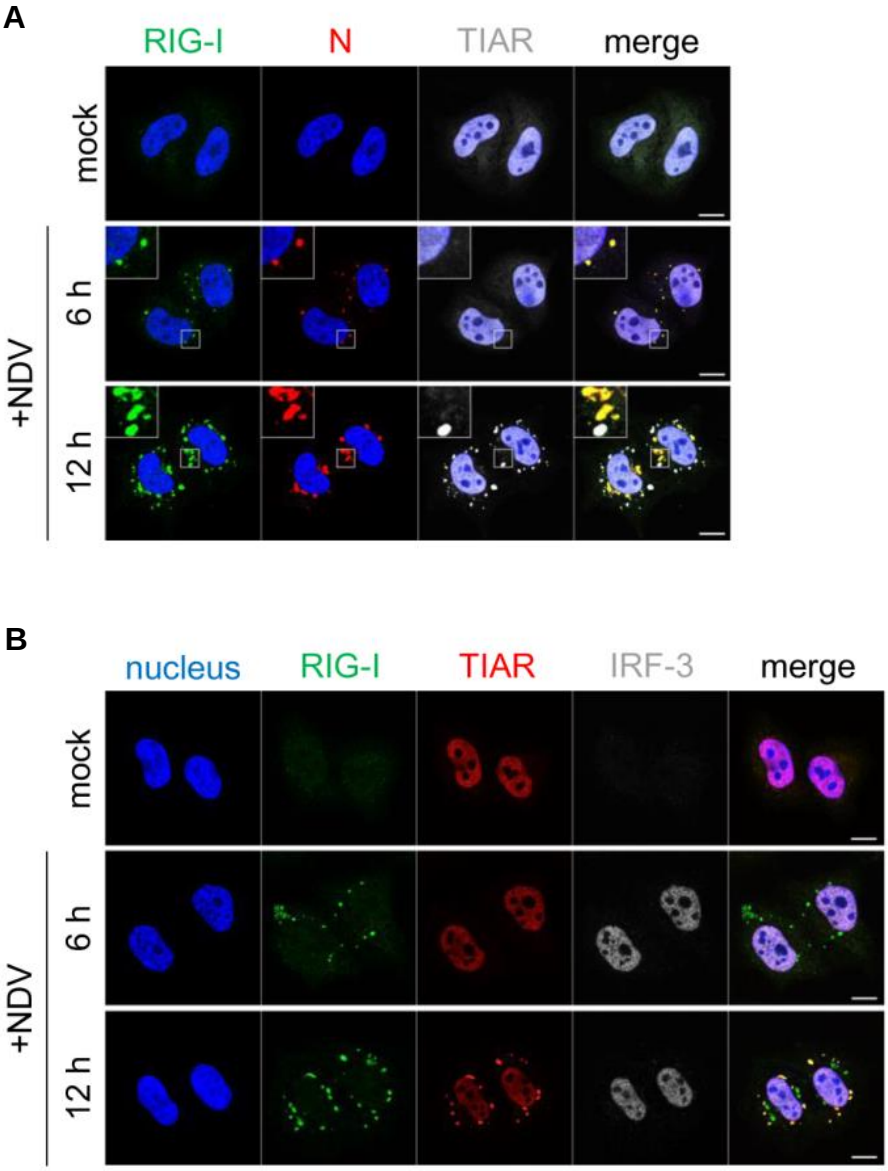

Figure 3-10. RIG-I localization in NDV-infected cells

(A and B) HeLa cells were either mock treated or infected with NDV (MOI = 1) for 6 and 12 hours. Cells were immunostained for RIG-I (green), N (red), and TIAR (white) (A), or RIG-I (green), TIAR (red), and IRF-3 (white) (B). Nuclei were stained with DAPI (blue). The white scale bar corresponds to 10 μm. The boxed area was enlarged and displayed on the left.

3-6. IPS-1 associated with both NDV vRCs and avSGs

RIG-I transduces its signal to the downstream adaptor, IPS-1, which is expressed on the mitochondrial outer membrane. I further monitored the localization of IPS-1 using HeLa cells stably expressing FLAG-tagged IPS-1 [12] upon NDV infection. At 6 hpi, IPS-1 localized in the proximity of vRCs, showing a yellow color in the periphery of vRCs (as shown by L), suggesting their close interaction (Figure 3-11A). At 12 hpi, avSGs were clearly detected and partially co-localized with IPS-1 (Fig 3-11A, bottom right). I also confirmed the interaction of endogenous IPS-1 with both vRCs and avSGs (Figure 3-11B). This data strongly suggests that IPS-1 was communicates with RIG-I associated with both vRCs and avSGs for signal transduction.

3-7. Dissociation of IPS-1 from NDV vRCs/avSGs impaired *IFNB* gene induction

Since microtubules have been shown to drive the arrangement of mitochondria [34], and SGs are known to translocate on the microtubule network [35], I assumed that the disruption of microtubules affected the dynamics of IPS-1 and might dissociate its interaction with vRCs and avSGs. I treated HeLa cells with nocodazole, which disrupts the organization of microtubules. The nocodazole treatment in uninfected cells did not induce significant changes in the morphology of mitochondria, as determined by staining for FLAG-IPS-1 (Figure 3-12A, upper). In NDV-infected cells without the treatment, FLAG-IPS-1 partially merged with both vRCs/avSGs as observed with the yellow interface (Figure 3-12A, lower). The nocodazole treatment clearly impaired these interactions, as judged by the disappearance of the interface. *IFNB* gene

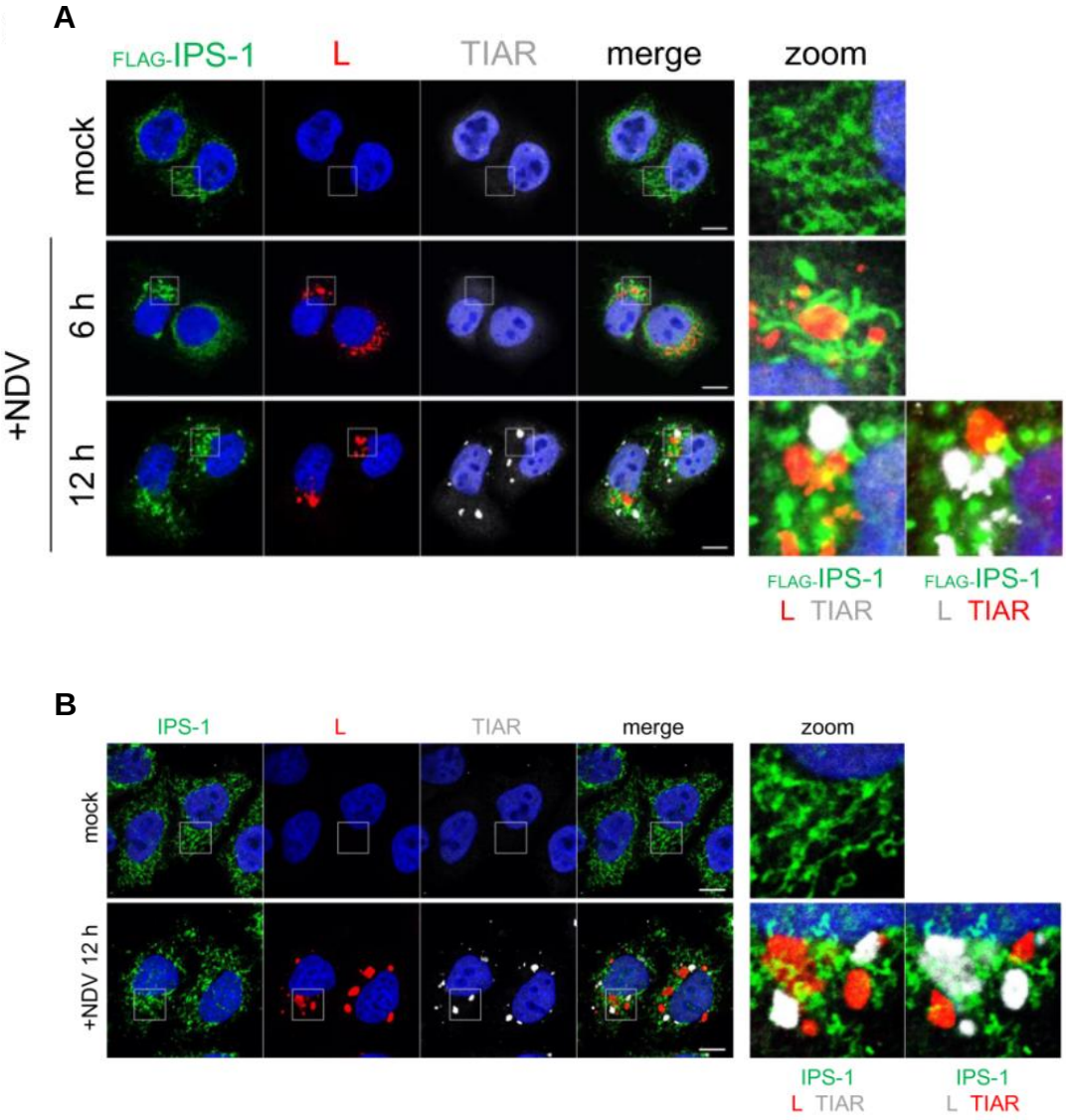

Figure 3-11. IPS-1 localization in NDV-infected cells

(A and B) FLAG-IPS-1/HeLa and HeLa cells were either mock treated or infected with NDV (MOI = 1) for 6 and 12 hours. The cells were immunostained for FLAG (green in A), IPS-1 (green in B), L (red), and TIAR (white). Nuclei were stained with DAPI (blue). The white scale bar corresponds to 10 μm. The boxed area was enlarged and is displayed on the right (zoom). Partial co-localization between IPS-1 and L (vRC) or TIAR (avSG) is shown by displaying them in green and red, respectively (zoom).

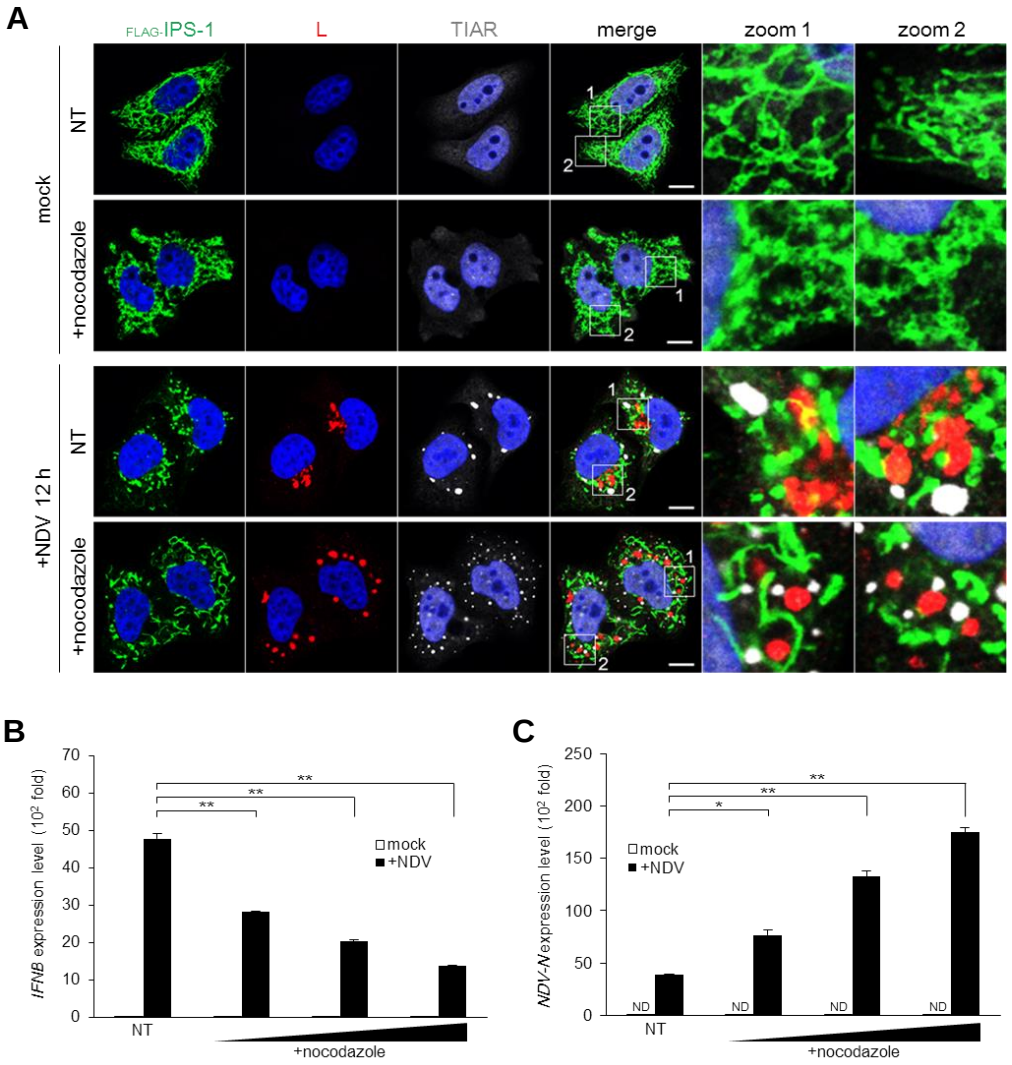

Figure 3-12. Nocodazole treatment for the inhibition of IPS-1 dynamics

(A) FLAG-IPS-1/HeLa cells were mock treated (NT) or treated with 10 μg/μl of nocodazole for 1 hour. After the treatment, the cells were mock treated or infected with NDV (MOI = 1) for 12 hours and immunostained for FLAG (green), L (red), and TIAR (white). Nuclei were stained with DAPI (blue). The white scale bar corresponds to 10 μm. The two boxed areas in the merged image were enlarged and are shown on the right (zoom 1 and 2). **(B and C)** FLAG-IPS-1/HeLa cells were mock treated (NT) or treated with 0.625, 2.5, or 10 μg/μl of nocodazole for 1 hour followed by mock or NDV infection (MOI = 1) for 12 hours. Expression levels of *IFNB* mRNA (B) and NDV-N RNA (C) were quantified by RT-qPCR. Data is represented as means of ±SD (t-test: ***p<0.01, **p<0.05, *p<0.1, NS = not significant). ND = not detectable.

expression induced by NDV was dose-dependently impaired by nocodazole (Figure 3-12B), strongly suggesting that the observed interface was physiologically relevant. Conversely, NDV replication was dose-dependently increased by nocodazole, thereby excluding the possibility that the treatment attenuated the expression of *IFNB* by inhibiting viral replication (Figure 3-12C). Takeing these observations together, I hypothesized that RIG-I initially accumulated in NDV vRCs to undertake primary IFN induction, and subsequently translocated to avSGs to boost a strong secondary IFN production in the later phase. In each case, IPS-1 mediated RIG-I-triggered signaling by closely associating with RIG-I within both granules.

3-8. avSGs were required for full activation of *IFNB* gene expression

To elucidate the significance of avSGs in *IFNB* gene expression further, I blocked SGs formation. I knocked down the expression of PKR, which acts as a sensor for viral infection and triggers avSG formation [58]. I also targeted G3BP proteins (G3BP1 and G3BP2: G3BPs), which are critical for SG assembly and its maintenance [55, 63, 66]. I knocked down RIG-I for comparison. A western blot analysis confirmed efficient knockdown of target genes (Figure 3-13A). These cells were infected with NDV and *IFNB* gene expression was examined by RT-qPCR (Figure 3-13B). As expected, the knockdown of RIG-I impaired *IFNB* gene expression and the treatment with siPKR or siG3BPs also inhibited *IFNB* gene induction. The kinetics of vRCs, avSGs, and *IFNB* mRNA induction were subsequently examined in these cells (Figure 3-13C). These results were quantified as in Figure 3-8 (Figure 3-14). In control cells at 12 hpi, vRCs were observed in almost all cells (light gray + black, 97-99%) (Figure 3-14A).

Knockdown of RIG-I, PKR or G3BPs did not decrease the number of vRCs-positive cells (Figure 3-14B-D, light gray + black,). The knockdown of RIG-I markedly blocked *IFNB* mRNA expression (red + green, 56.1 to 8.2% at 12 hpi) (Figure 3-15B); however, the number of avSGs-positive cells remained constant (black, 91.4 to 83.8% at 12 hpi) (Figure 3-14B). The knockdown of PKR strongly inhibited the formation of avSGs (black, 91.4 to 17.9% at 12 hpi) (Figure 3-14C) and decreased the number of *IFNB* mRNA-positive cells (red + green, 56.1 to 18.4% at 12 hpi) (Figure 3-15C). The knockdown of G3BPs also inhibited avSGs (black, 91.4 to 21.7% at 12 hpi) (Figure 15D) and decreased the number of *IFNB* mRNA-positive cells (red + green, 56.1 to 21.8% at 12 hpi) (Figure 3-15D). Concomitant with the inhibition of avSGs, the number of cells exhibiting vRCs and *IFNB* mRNA increased, suggesting that these cells failed to develop into triple-positive, high *IFNB* gene-expressing cells (Figure 3-16C and D). I also examined the expression of ISGs; *ISG20*, *ISG56*, and *CXCL10* genes by RT-qPCR at 12 hpi (Figure 3-16). The expression of these genes was dependent on RIG-I, PKR, and G3BPs. These results strongly suggested that avSGs contributed to the robust *IFNB* gene expression observed at approximately 12 hpi.

3-9. Viral poly(A)$^+$ RNA stimulated *IFNB* induction

I observed that avSGs contained vRNA(+), but not vRNA(-) (Figure 3-3) nor vdsRNA (Figure 3-5). I suspected that vRNA(+) activated RIG-I in avSGs, culminating in *IFNB* gene expression at 12 hpi. vRNA(+) consists of viral mRNA (vmRNA) containing 3'-poly(A) tail and viral anti-genomic complementary RNA (vcRNA), a template RNA for vgRNA synthesis during viral replication. Since vmRNA is a major

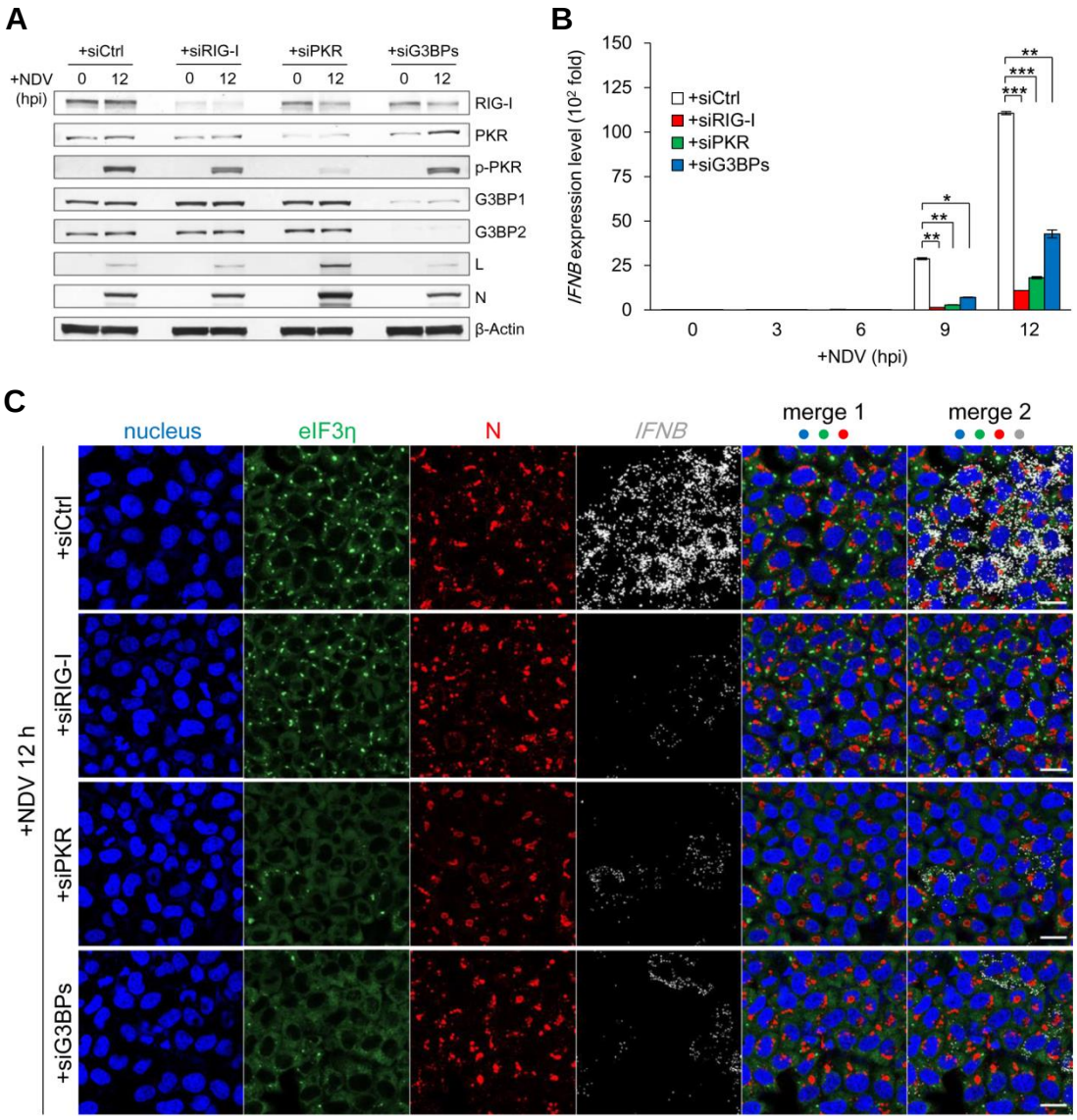

Figure 3-13. Gene knockdown for the inhibition of avSGs formation

(A-C) HeLa cells were transfected with siRNAs; siCtrl, siRIG-I, siPKR, or siG3BPs (for G3BP1 and G3BP2). After transfection, the cells were infected with NDV (MOI = 1) for the indicated time. (A) Expression levels of the indicated proteins were analyzed by western blotting. (B) *IFNB* mRNA expression was analyzed by RT-qPCR. Data is represented as means of ±SD (t-test: ***p<0.01, **p<0.05, *p<0.1, NS = not significant). **(C)** Cells were immunostained for eIF3η (green) and N (red). *IFNB* mRNA (white) was detected by the RNA-FISH method. Nuclei were stained with DAPI (blue). Merge 1: nuclei, eIF3η, N. Merge 2: nuclei, eIF3η, N, and *IFNB* mRNA. The white scale bar corresponds to 20 μm).

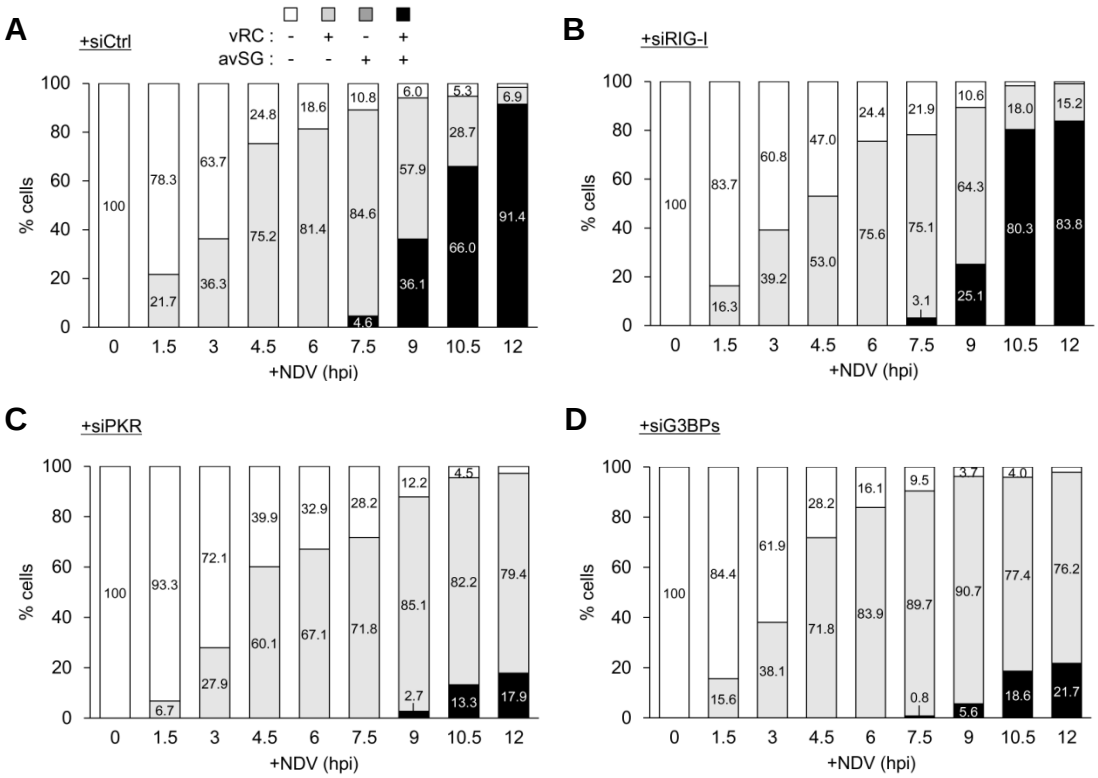

Figure 3-14. Quantification of vRCs/avSGs in avSG-blocked cells

(A-D) HeLa cells were transfected with siRNAs; siCtrl, siRIG-I, siPKR, or siG3BPs (siG3BP1 and siG3BP2). After transfection, the cells were infected with NDV (MOI = 1) for the indicated time up to 12 hours. Three hundred cells at each time point of infection were counted by MetaMorph software. Cells were categorized according to the existence of vRCs and avSGs as shown above. Percentages are indicated inside the data bar.

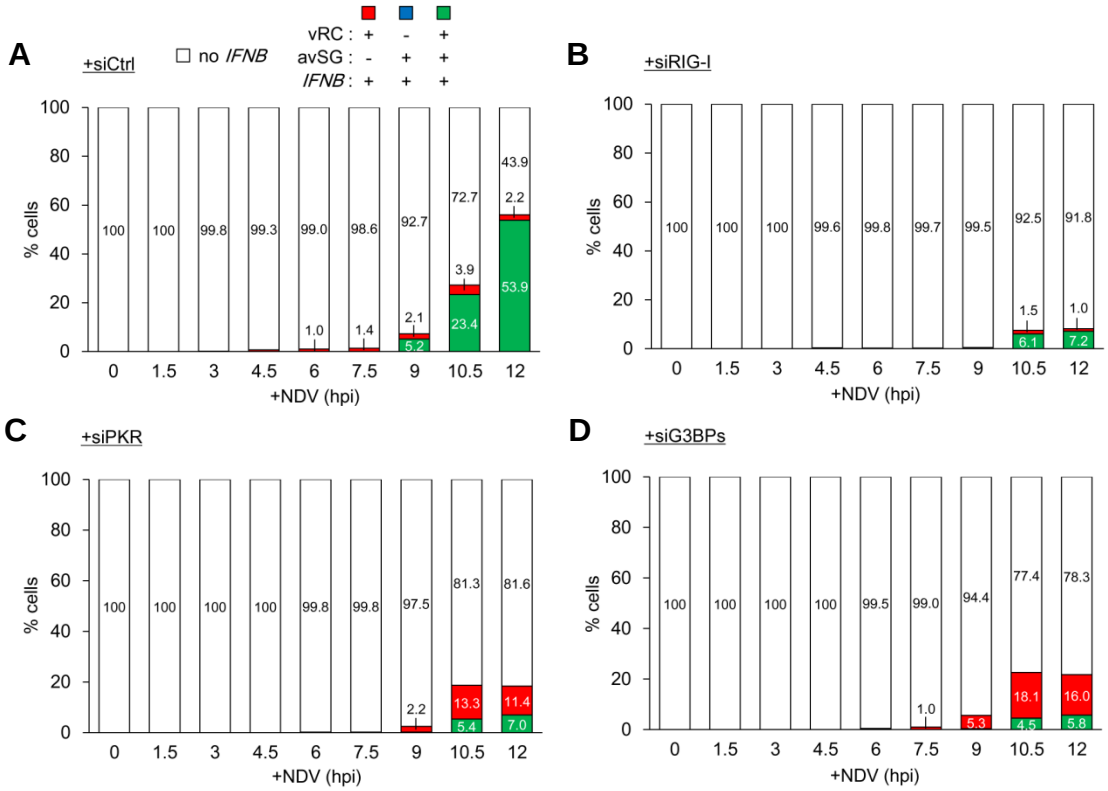

Figure 3-15. Quantification of *IFNB* mRNA expression in avSGs-blocked cells

(A-D) HeLa cells were transfected with siRNAs; siCtrl, siRIG-I, siPKR, or siG3BPs (siG3BP1 and siG3BP2). After transfection, the cells were infected with NDV (MOI = 1) for the indicated time up to 12 hours. Three hundred cells at each time point of infection were counted by MetaMorph software. Cells were categorized according to the existence of vRCs, avSGs, and *IFNB* mRNA as shown above. Percentages are indicated inside the data bar.

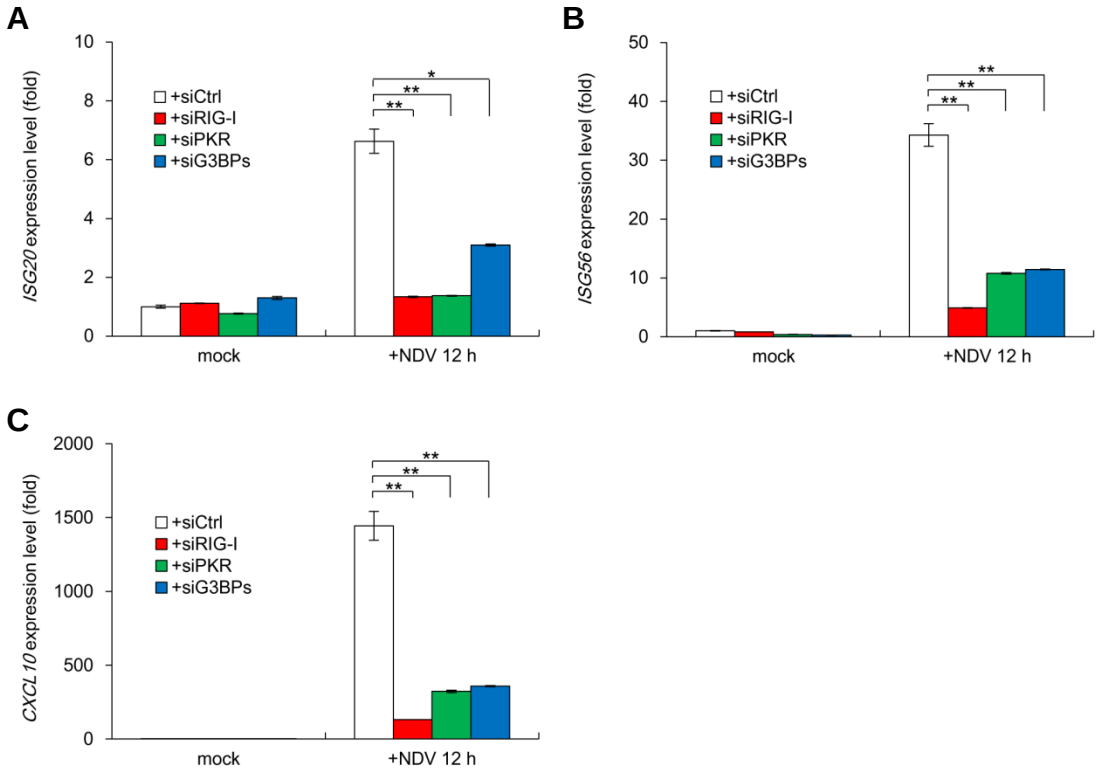

Figure 3-16. ISGs induction in avSGs-blocked cells

(A-C) HeLa cells were transfected with siRNAs; siCtrl, siRIG-I, siPKR, or siG3BPs (siG3BP1 and siG3BP2). After transfection, the cells were mock treated or infected with NDV (MOI = 1) for 12 hours. Expression levels of *ISG20*, *ISG56*, and *CXCL10* mRNA were measured by qRT-PCR. Data is represented as means of ±SD (t-test: ***p<0.01, **p<0.05, *p<0.1, NS = not significant).

part of RNA that constitutes vRNA(+), I considered whether NDV poly(A)$^+$ vmRNA could be a potent activator of *IFNB* gene expression in avSGs. To obtain vmRNA, I isolated total RNA from NDV-infected HeLa cells and fractionated into poly(A)$^+$ and poly(A)$^-$ RNA populations using oligo(dT)-combined latex beads (Figure 3-17). These RNA fractions were tested for the induction of *Ifnb* mRNA in mouse embryonic fibroblasts (MEFs). RNA fractions extracted from uninfected cells did not activate the *Ifnb* gene (Figure 3-18A), whereas both poly(A)$^+$ and poly(A)$^-$ RNA extracted from NDV-infected cells exhibited strong *Ifnb*-inducing activity. In addition to *Ifnb*, *Isg56* and *Cxcl10* genes were also activated by these RNA fractions (Figure 3-19). I further tested other viruses belonging to *Mononegavirales*, RSV (Figure 3-18B) and VSV (Figure 3-18C). The results revealed that poly(A)$^+$ RNA from RSV and VSV also exhibited strong stimulatory activity, suggesting that poly(A)-containing viral transcripts of the *Mononegavirales* viruses potentially activates antiviral innate immunity.

3-10. NDV poly(A)$^+$ RNA formed double-stranded, 5’-triphosphate structure

To further characterize the structural feature of the immunostimulatory NDV poly(A)$^+$ RNA, the poly(A)$^+$ RNA fraction from NDV-infected HeLa cells was treated with RNase III, CIAP, or DNase I. *Ifnb* and ISGs induction were dramatically impaired by RNase III or CIAP, but not by the DNase I treatment (Figure 3-20A and 3-21), suggesting that the stimulatory activity resides in poly(A)$^+$ RNA species which formed a secondary structure and end-phosphate moieties, such as 5’-triphosphate. To examine the presence of 5'-triphosphate in the stimulatory RNA, the NDV poly(A)$^+$ RNA

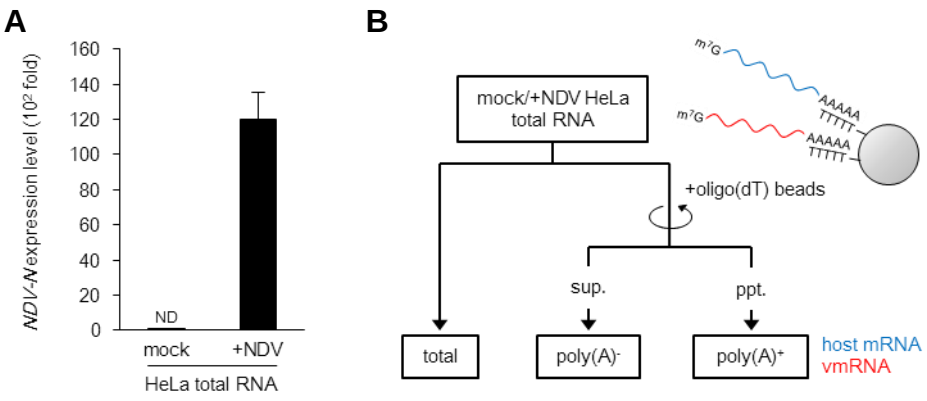

Figure 3-17. Isolation of NDV poly(A)$^+$ RNA

(A) NDV viral RNA (*NDV-N*) expression level in the mock and NDV-infected (MOI = 1) HeLa total RNA was measured by RT-qPCR. Data is represented as means of ±SD. ND = not detected. **(B)** Experimental scheme of poly(A)$^+$ RNA isolation. Total RNA of mock/NDV-infected (MOI = 1) HeLa cells was incubated with oligo(dT)-combined latex beads. By centrifugation, supernatant and precipitate were separated for the poly(A)$^-$ and poly(A)$^+$ RNA fraction respectively.

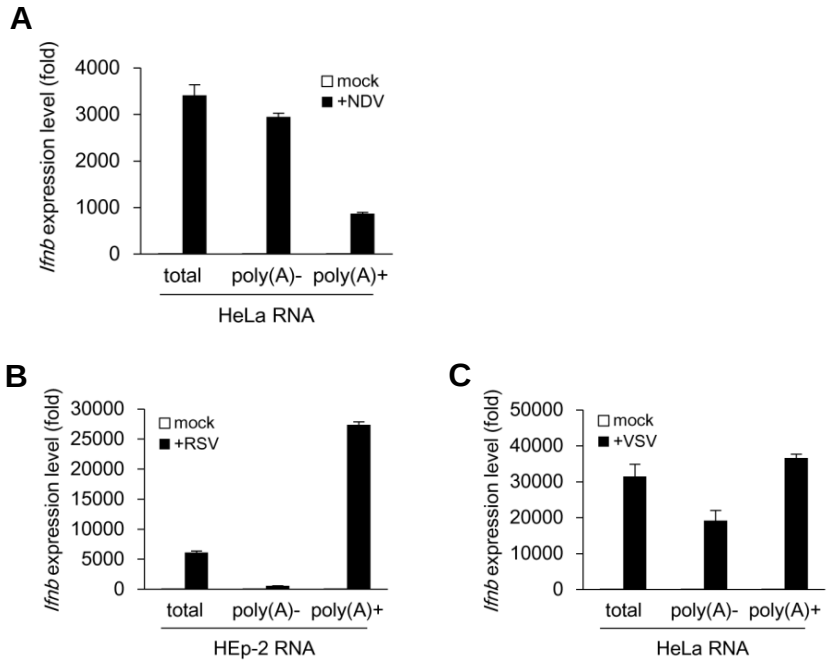

Figure 3-18. *Ifnb* activation by poly(A)$^+$ viral RNAs from *Mononegavirales*

(A-C) Total RNA of mock treated or NDV-infected (12 hpi, MOI = 1) HeLa cells (A), RSV-infected (60 hpi, MOI = 1) HEp-2 cells (B), or VSV-infected (12 hpi, MOI = 1) HeLa cells (C) was separated into the poly(A)$^-$ and poly(A)$^+$ RNA fractions by oligo(dT)-combined latex beads and transfected into MEFs (1×10^5 cells were transfected with 200 ng RNA). *Ifnb* mRNA expression levels were measured by RT-qPCR. Data is represented as means of ±SD.

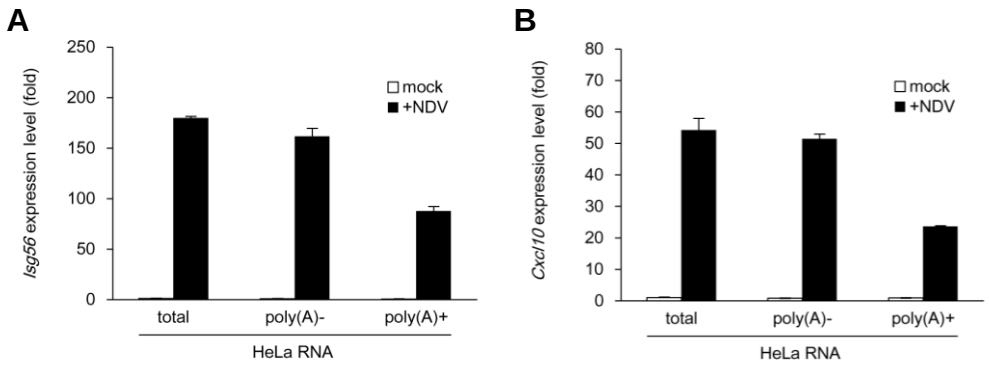

Figure 3-19. ISGs induction by NDV poly(A)$^+$ RNA

(A and B) MEFs (2×10^5 cells) were transfected with total, poly(A)$^-$, or poly(A)$^+$ RNA (200 ng) from mock/NDV-infected (MOI = 1) HeLa cells. *Isg56* and *Cxcl10* mRNA expression levels were measured by RT-qPCR. Data is represented as means of ±SD.

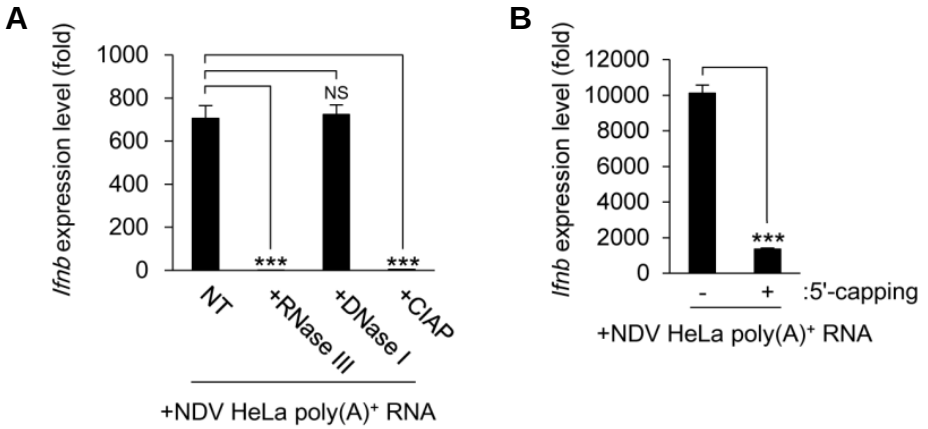

Figure 3-20. *Ifnb*-inducing activity of enzyme-treated NDV poly(A)$^+$ RNA

(A and B) The poly(A)$^+$ RNA fraction from NDV-infected (12 hpi, MOI = 1) HeLa cells was mock treated (NT) or treated with RNase III, DNase I, CIAP (D), or the 5'-capping enzyme of Vaccinia virus (E) and then transfected to MEFs (1×10^5 cells were transfected with 200 ng RNA). *Ifnb* mRNA expression levels were measured by RT-qPCR. Data is represented as means of ±SD (t-test: ***p<0.01, NS = not significant).

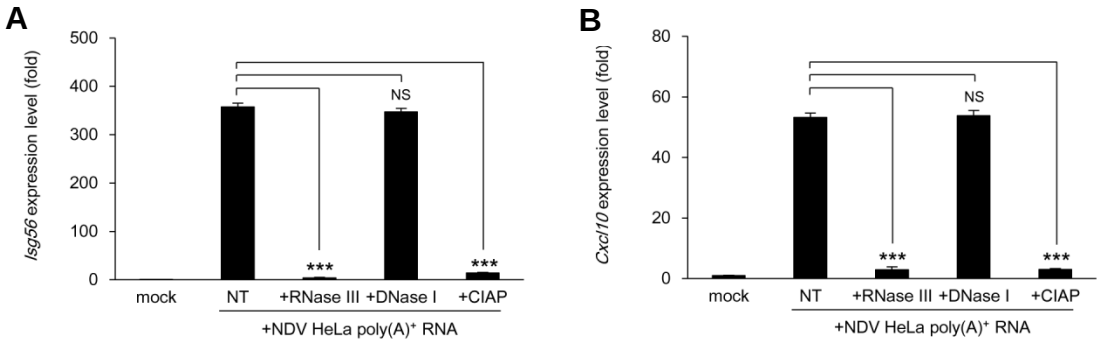

Figure 3-21. ISGs induction by NDV poly(A)$^+$ viral RNA

(A and B) The poly(A)$^+$ RNA fraction from NDV-infected (12 hpi, MOI = 1) HeLa cells was mock treated (NT) or treated with RNase III, DNase I, CIAP (D), or the 5'-capping enzyme of Vaccinia virus (E) and then transfected to MEFs (1×10^5 cells were transfected with 200 ng RNA). *Ifnb* mRNA expression levels were measured by RT-qPCR. Data is represented as means of ±SD (t-test: ***p<0.01, NS = not significant).

fraction was further subjected to reaction with the capping enzyme of vaccinia virus, which adds a cap to the 5'-triphosphate end. The capping reaction diminished the *Ifnb* gene induction by the RNA (Figure 3-20B), therefore I speculated that the stimulatory activity of NDV poly(A)$^+$ RNA was from the remaining 5'-triphosphate-containing RNA.

3-11. NDV produced read-through transcript

Transcription of NDV occurs in the order 3'-Le-N-P-M-F-HN-L-Tr-5'. The first transcript Le possesses a 5'-triphosphate and is devoid of a 3'-poly(A). However, transcripts for N, P, M, F, HN and L possess both a 5'-cap and 3'-poly(A). I analyzed viral N mRNA by strand-specific northern blotting (Figure 3-22A). RNA extracted from NDV-infected HeLa cells was fractionated into poly(A)$^+$ and poly(A)$^-$ populations. Ethidium bromide staining revealed the virtual absence of ribosomal RNA in the poly(A)$^+$ RNA fraction, demonstrating successful fractionation (Figure 3-22A, bottom). As expected, the northern analysis with a N-specific RNA probe revealed that N mRNA (1.7 kilonucleotides, knt) was enriched in the poly(A)$^+$ RNA fraction (Figure 3-22A, top). Interestingly, this probe detected additional slow migrating RNA at 3.8 knt. I suspected that this larger RNA was read-through N mRNA, an extended transcript covering the N and P genes [67]. Indeed, many types of viruses belonging to *Mononegavirales* have been shown to produce read-through transcripts [68-70].

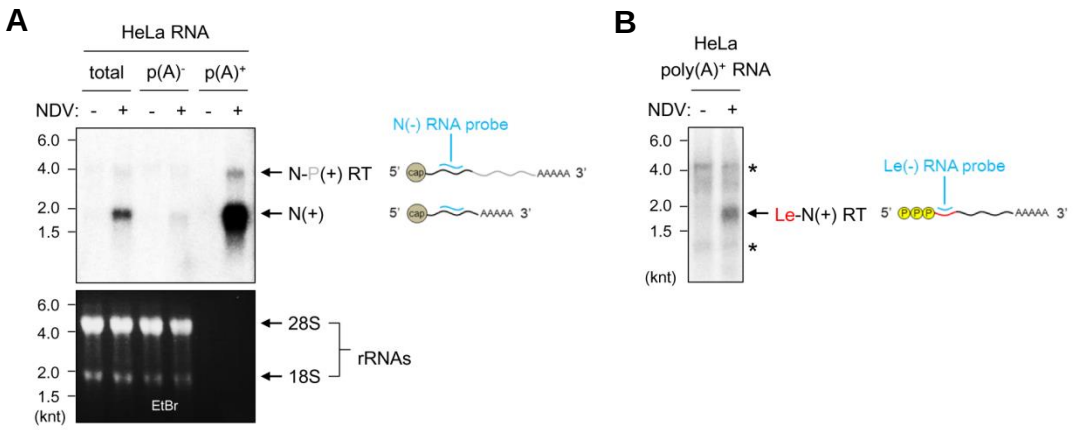

Figure 3-22. Strand-specific northern blotting for NDV poly(A)$^+$ RNA

(A) Total, poly(A)$^-$, and poly(A)$^+$ RNA (each 250 ng) from mock treated or NDV-infected (12 hpi, MOI = 1) HeLa cells were separated on a denaturing agarose gel. An ethidium bromide (EtBr)-stained gel is shown at the bottom. vRNA(+) was detected by blotting with an N-specific RNA probe (N(-)). Positions of N vmRNA (N(+)) and N-P read-through RNA (N-P(+) RT) are shown. knt = kilo nucleotide. RNA probe and target vRNA(+) are illustrated alongside the results. **(B)** The poly(A)$^+$ RNA from mock treated or NDV-infected (12 hpi, MOI = 1) HeLa cells was subjected to strand-specific northern blotting using a leader-specific RNA probe (Le(-)). The position of Le-N read-through RNA is shown (Le-N(+) RT). *non-specific band. The RNA probe and target vRNA(+) are illustrated alongside the results.

3-12. NDV, RSV, and VSV produced leader-containing read-through RNA

I further examined the presence of Le-N read-through transcript, because such an RNA possesses both 5'-triphosphate and 3'-poly(A) [69]. To detect Le-N read-through RNA, I performed strand-specific northern analysis using Le-specific RNA probe (Figure 3-22B). Poly(A)$^+$ RNA from NDV-infected cells exhibited 1.7 knt signal by this probe. Le RNA (55 nt) was undetectable in this gel due to its small size. To quantify Le-N read-through RNA, we used a protocol for strand-specific RT-qPCR [65]. This method provided specific detection of the target RNAs (Figure 3-23A). First, I quantified the positive-strand Le-N sequence (Figure 3-24A). As expected, the Le-N was enriched in the poly(A)$^+$ fraction. Next, I quantified the negative-strand Le-N sequence to exclude the possibility that the stimulatory activity is from vmRNA partially hybridized with negative-strand vdRNA (Figure 3-24B). The result revealed that negative-strand Le-N sequence was hardly detectable in the poly(A)$^+$ fraction, excluding the possibility mentioned above. Interestingly, this technique demonstrated similar read-through transcripts (Le-NS1, RSV; Le-N, VSV) in cells infected with RSV and VSV (Figure 3-23B, C, and 3-25), suggesting common potential immunostimulatory activity of Le-N read-through transcript produced by the *Mononegavirales* viruses.

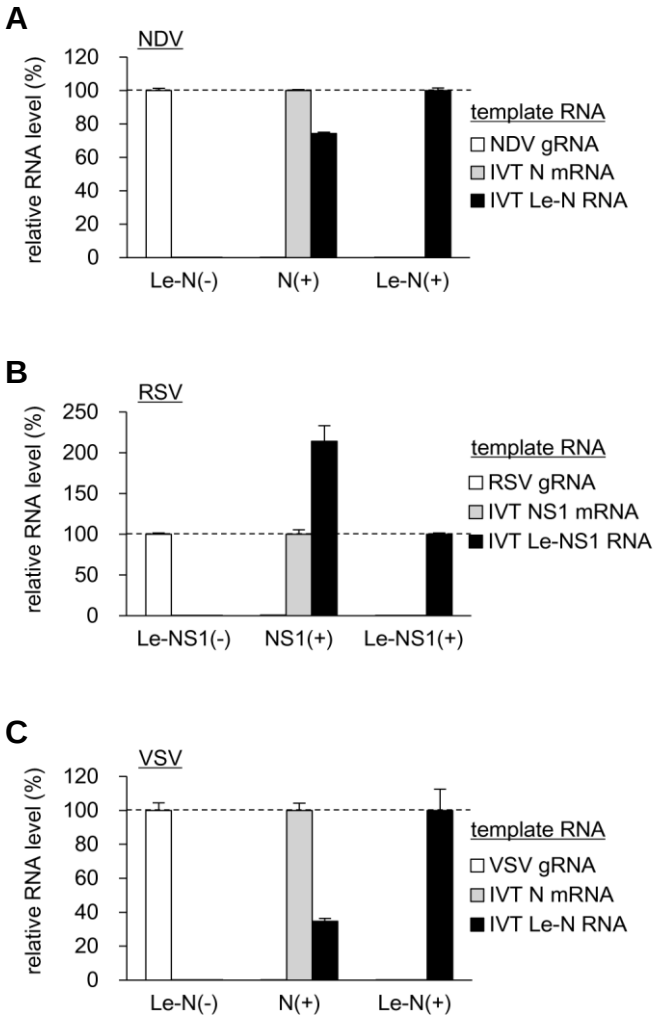

Figure 3-23. Validation of strand-specific RT-qPCR

(A-C) 10^{10} copies of vgRNA isolated from the viral particles and *in vitro*-synthesized RNA (IVT RNA) corresponding to vmRNA (N, NS1 and N for NDV, RSV and VSV, respectively) and read-through RNA (Le-N, Le-NS1 and Le-N for NDV, RSV and VSV, respectively) were subjected to strand-specific RT-qPCR (ssRT-qPCR) using specific primer sets (Table 3-2, 3-3, and 3-4). Percentage of the RNA copies of each target RNA is shown. Data is represented as means of ± SD. The results show the specificity of ssRT-qPCR: the probe for vRNA(-) only detected vgRNA; the probe for Le-N/NS1(+) read-through RNA selectively detected Le-N/NS1 RNA but not N mRNA.

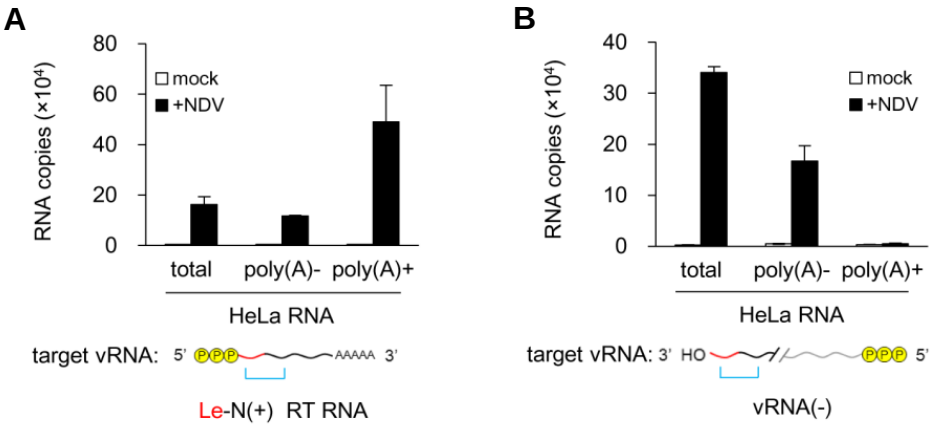

Figure 3-24. Strand-specific RT-qPCR for NDV poly(A)$^+$ RNA

(A and B) Total, poly(A)$^-$, and poly(A)$^+$ RNA (each 200 ng) from mock treated or NDV-infected (12 hpi, MOI = 1) HeLa cells were subjected to strand-specific RT-qPCR (ssRT-qPCR) targeting Le-N(+) read-through RNA (A) or targeting vRNA(-) (B). Primers used are listed in Table 3-2. Data is represented as means ±SD. Target vRNAs in the assay are illustrated below.

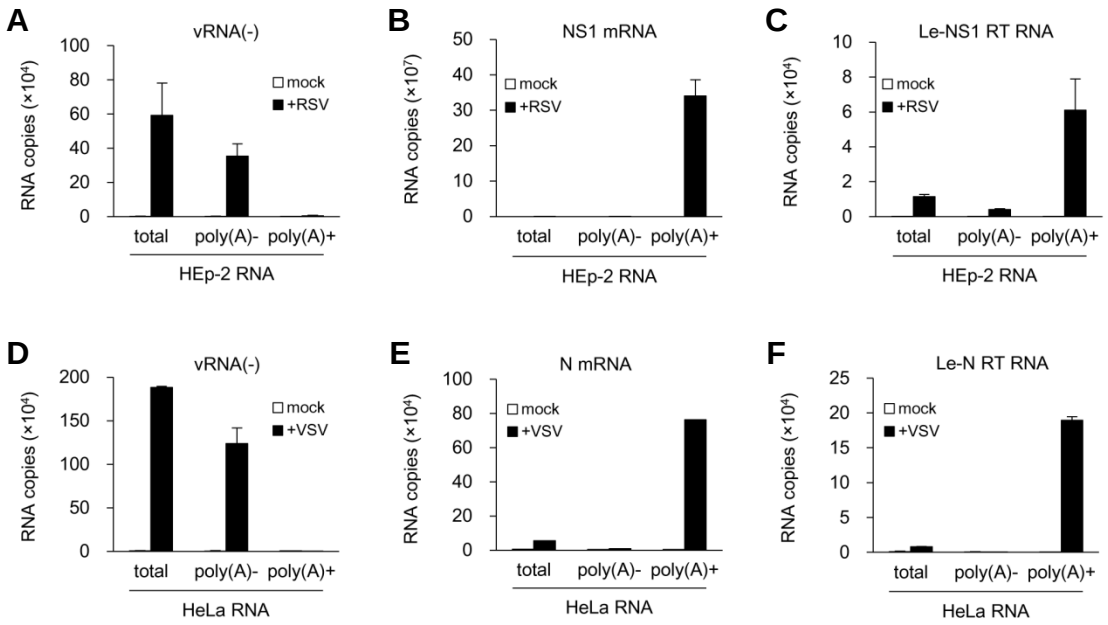

Figure 3-25. Strand-specific RT-qPCR analysis for RSV and VSV vRNAs

(A-F) Total, poly(A)$^-$, and poly(A)$^+$ RNA from mock treated, RSV-infected (60 hpi, MOI = 1) HEp-2 cells (A-C), or VSV-infected (12 hpi, MOI = 1) HeLa cells (D-F) were subjected to strand-specific RT-qPCR (ssRT-qPCR) targeting Le-NS1/N(-) as a portion of vgRNA, NS1/N(+) vmRNA, and Le-NS1/N(+) read-through RNA with specific primer sets (Table 3-3 and 3-4). Data is represented as means of ±SD.

Table 3-1. Primers used for *in vitro* transcription

Virus	vRNA	Primer Name	Sequence (5'-3')
NDV	Le(-)	Le(+)1F	accaaacagagaatcggtga
		T7-Le(-)55R	TAATACGACTCACTATAGGGgcgacttcaattgctccttc
	Le(+)	T7-Le(+)1F	TAATACGACTCACTATAGGGaccaaacagagaatcggtga
		Le(-)55R	gcgacttcaattgctccttc
	N(-)	N(+)746F	ctctaccccgtatgcaggag
		T7-N(-)892R	TAATACGACTCACTATAGGGtgagtccacgtcccctacta
	N(+)	T7-Le(+)56F	TAATACGACTCACTATAGGGacgggtagaaggtgtgaatctcgagtgcga
		N(-)1801R	ttttttctaattccctcggctctgttttga
	Le-N(+)	T7-Le(+)1F	TAATACGACTCACTATAGGGaccaaacagagaatcggtga
		N(-)1801R	ttttttctaattccctcggctctgttttga
RSV	NS1(+)	T7-Le(+)45F	TAATACGACTCACTATAGGGggggcaaataagaatttgataagtaccact
		N(-)576R	ttttatattaactaatggtgctagtgacattg
	Le-NS1(+)	T7-Le(+)1F	TAATACGACTCACTATAGGGacgcgaaaaaatgcgtacaa
		N(-)576R	ttttatattaactaatggtgctagtgacattg
VSV	NS1(+)	T7-Le(+)51F	TAATACGACTCACTATAGGGggggcaaataagaatttgataagtaccact
		N(-)1383R	ttttatattaactaatggtgctagtgacattg
	Le-NS1(+)	T7-Le(+)1F	TAATACGACTCACTATAGGGacgcgaaaaaatgcgtacaa
		N(-)1383R	ttttatattaactaatggtgctagtgacattg

Table 3-2. Primer sets used for ssRT-qPCR targeting NDV vRNAs

Target		Primer Name	Sequence (5'-3')	Use
NDV vRNA	Strand			
N	(+)	mTag-N(-)286R	CCAGATCGTTCGAGTCGTgcagaataccgcaaagttcc	RT
		mTag	CCAGATCGTTCGAGTCGT	qPCR
		N(+)122F	atgtcgtccgtatttgacga	qPCR
Leader-N	(-)	gTag-Le(+)1F	GGCCGTCATGGTGGCGAATaccaaacagagaatcggtga	RT
		gTag	GGCCGTCATGGTGGCGAAT	qPCR
		N(-)286R	gcagaataccgcaaagttcc	qPCR
	(+)	mTag-N(-)286R	CCAGATCGTTCGAGTCGTgcagaataccgcaaagttcc	RT
		mTag	CCAGATCGTTCGAGTCGT	qPCR
		Le(+)1F	accaaacagagaatcggtga	qPCR

Table 3-3. Primer sets used for ssRT-qPCR targeting RSV vRNAs

Target		Primer Name	Sequence (5'-3')	Use
RSV vRNA	Strand			
NS1	(+)	mTag-N(-)286R	CCAGATCGTTCGAGTCGTctacttgtaataacatgcac	RT
		mTag	CCAGATCGTTCGAGTCGT	qPCR
		NS1(+)99F	atgggcagcaattcgttgag	qPCR
Leader-NS1	(-)	gTag-Le(+)1F	GGCCGTCATGGTGGCGAATacgcgaaaaaatgcgtacaa	RT
		gTag	GGCCGTCATGGTGGCGAAT	qPCR
		NS1(-)286R	ctacttgtaataacatgcac	qPCR
	(+)	mTag-N(-)286R	CCAGATCGTTCGAGTCGTctacttgtaataacatgcac	RT
		mTag	CCAGATCGTTCGAGTCGT	qPCR
		Le(+)1F	accaaacagagaatcggtga	qPCR

Table 3-4. Primer sets used for ssRT-qPCR targeting VSV vRNAs

Target		Primer Name	Sequence (5'-3')	Use
VSV vRNA	Strand			
N	(+)	mTag-N(-)286R	CCAGATCGTTCGAGTCGTtacaagtagctgttgacatg	RT
		mTag	CCAGATCGTTCGAGTCGT	qPCR
		N(+)64F	atgtctgttacagtcaagag	qPCR
Leader-N	(-)	gTag-Le(+)1F	GGCCGTCATGGTGGCGAATaccaaacagagaatcggtga	RT
		gTag	GGCCGTCATGGTGGCGAAT	qPCR
		N(-)286R	gcagaataccgcaaagttcc	qPCR
	(+)	mTag-N(-)286R	CCAGATCGTTCGAGTCGTgcagaataccgcaaagttcc	RT
		mTag	CCAGATCGTTCGAGTCGT	qPCR
		Le(+)1F	accaaacagagaatcggtga	qPCR

3-13. *In vitro* Le-N RNA induced *IFNB* gene expression and SGs formation

Finally, I synthesized the RNA corresponding to Le and the Le-N read-through RNA *in vitro*, and examined their immunostimulatory activity (Figure 26A). The *in vitro* products of Le-N read-through RNA with 3'-poly(A) as well as Le RNA were capable of inducing *IFNB* gene activation. I also monitored Cy3-labeled Le-N read-through RNA with 3'-poly(A) after transfection. I observed that this RNA induced the formation of SGs containing G3BP1 and Cy3 signal, and partially co-localized with SGs (Figure 3-26B). Here, Cy3 signal did not completely coincided with SGs, presumably because most Cy3-RNA resided within endosomes and a portion of the RNA escaped into the cytoplasm and induced SGs. The results strongly suggest that viral Le-N read-through transcript is quite capable of inducing avSGs formation followed by induction of *IFNB* gene via RIG-I signaling.

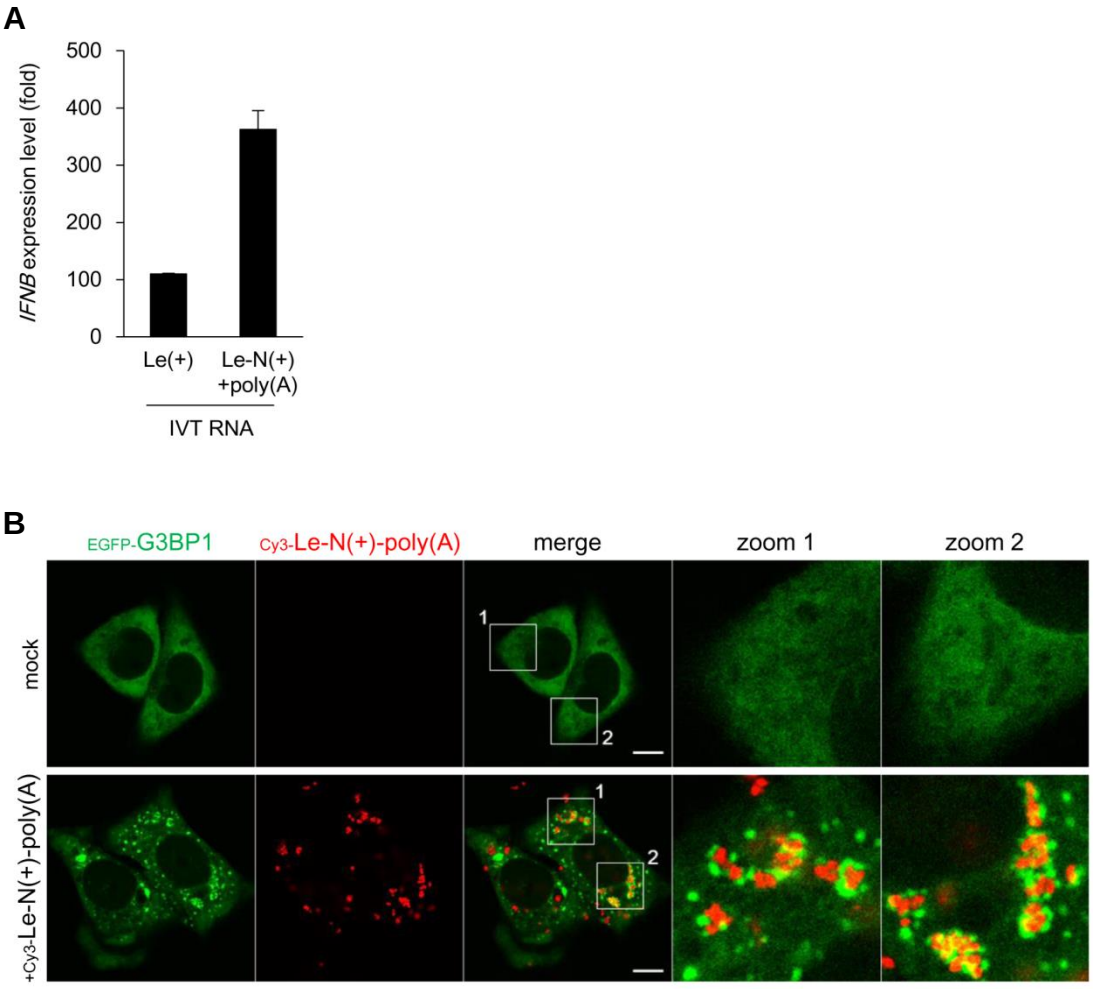

Figure 3-26. *IFNB* gene and SGs induction by *in vitro*-transcribed Le-N RNA

(A) RNA corresponding to NDV Le RNA (Le(+)) and Le-N read-through RNA (Le-N(+)+poly(A)) were synthesized *in vitro*. These RNA preparations (200 ng) were tested for *IFNB* gene expression by transfecting to FLAG-RIG-I/HeLa cells (2×10^5 cells). *IFNB* mRNA expression levels were measured by RT-qPCR. Data is represented as means of ±SD. **(B)** Cy3-labeled Le-N(+)+poly(A) (40 ng) was synthesized *in vitro* and transfected into EGFP-G3BP1/HeLa cells (0.25×10^5 cells). After 6 hours, cells were treated with 10 μM chloroquine for 1 hour to enhance transfection efficiency. Cells were fixed and visualized for EGFP-G3BP1 (green) and Cy3-labelled RNA (red). Enlarged images of boxed areas are shown (zoom 1 and 2).

4. Discussion

4-1. vRCs; a locale where RIG-I recognizes its authentic ligand, vgRNA

In this study, I aimed to figure out how RIG-I spatiotemporally encounters its RNA ligands and participates in cellular stress response upon NDV infection, which provokes a strong IFN response in mammalian cells. Immunostaining experiments and quantification analysis clearly demonstrated that NDV infection induced early generation of vRCs (1.5 hpi) and subsequent avSGs formation (7.5 hpi) (Figure 3-2, 3-7, and 3-8). RNA-FISH detection for NDV viral RNAs and *IFNB* mRNA further revealed that both NDV vRNA(-) and vRNA(+) localized in vRCs in the early phase (6 hpi) (Figure 3-3), when *IFNB* mRNA expression was already induced without avSGs (Figure 3-7 and 3-8). Importantly, RIG-I was detected in these early-formed vRCs along with IPS-1 aggregation (6 hpi), which is widely recognized as a hallmark of initiation of IFN induction [11, 12, 71] (Figure 3-11A). NDV vRNA(-) detected in vRCs is none other than vgRNA, which is considered to be a natural ligand of RIG-I [28]. Since purified NDV vgRNA activated *IFNB* gene expression in the transfected cells, and this activity was considerably abolished by RNase III and CIAP treatment (data not shown), NDV vgRNA supposedly forms a 5’-triphosphate dsRNA structure that corresponds to the well-studied archetype of RIG-I ligands [41, 44, 45, 49, 72]. It was obscure as to whether or not, as well as how, RIG-I encounters nucleoprotein-encapsidated vgRNA, as with NDV vRCs observed in this study. However, recent studies clearly demonstrated that RIG-I is accessible to 5’-triphosphate-dsRNAs within the incoming nucleocapsids of RNA viruses, such as IAV, VSV, Rift Valley fever virus, and La Crosse virus, to

provoke *IFNB* gene expression even in the absence of viral transcription and replication [73]. In the light of this information, this study provided ample evidence to define NDV vgRNA within primal vRCs as an authentic ligand of RIG-I. Therefore, vRCs are a primordial source of the immediate-early IFN production driven by the RIG-I/IPS1 signaling axis.

4-2. avSGs; a locale where RIG-I encounters sequestered viral poly(A)$^+$ RNA

To correlate the RIG-I-driven IFN-producing signaling with cellular stress response upon viral infection, I carefully investigated its kinetics along with avSGs formation. In line with previous reports [58, 59], the knockdown experiments in this study clearly explained the contribution of avSGs to substantial host IFN response against NDV infection (Figure 3-13, 3-15, and 3-16). Importantly, I discovered that NDV vRNA(+) that was initially derived from vRCs migrated to avSGs, and RIG-I also accumulated in avSGs along with IPS-1 (Figure 3-10 and 3-11). Meanwhile, I faced a critical question of whether NDV vRNA(+) induces *IFNB* gene expression via RIG-I, and the alternative of vmRNA or vcRNA to identify vRNA(+) in avSGs. Early studies fully described the physiological function of SGs as the regulatory machinery of host mRNA metabolism during environmental stresses: SGs sequester mRNA into a “safe shelter” composed of a variety of mRNA binding proteins [74]. In fact, many types of negative-strand RNA viruses including NDV produce 5’-capped and 3’-polyadenylated vmRNA as their transcripts, and no distinguishable signatures between viral and host mRNA have been unveiled so far. Thus, it was natural to presume that NDV poly(A)$^+$ vmRNA was internalized in avSGs together with host mRNA. I demonstrated that the poly(A)$^+$ RNA

fraction from NDV-infected HeLa cells contained NDV vmRNA, and was capable of stimulating *IFNB* gene expression and concomitant ISGs induction in MEFs (Figure 3-18, 3-19, and 3-22). However, host mRNA generally conforms to a certain format; therefore, it is not sensed as non-self. Since mRNA with m^7G-cap is not sensed by RIG-I, the acquisition of a cap is also a major strategy of viruses to escape immune detection. The importance of additional methylation adjacent to the cap has recently been reported [75, 76]. According to this theory, I suspected the presence of a novel immunostimulatory vmRNA species in avSGs. Intriguingly, treatment of NDV poly(A)$^+$ RNA fraction with RNase III, CIAP, and 5'-capping enzyme all resulted in significant loss of the ability to induce *IFNB* gene and ISGs expression (Figure 3-20 and 3-21). Therefore, it was convincing to conclude that NDV poly(A)$^+$ vmRNA within avSGs forms double-stranded and 5'-triphosphate structure, an eligible signature for an RIG-I ligand, and activated RIG-I and *IFNB* gene expression.

4-3. avSGs; a critical platform for the RIG-I sensing of multiple viral RNAs

Nonetheless, the viral RNA composition of avSGs observed in this study was different from IAV-induced avSGs, in which vgRNA was shown to be localized [58]. Moreover, avSGs induced by EMCV infection were previously reported to contained vdsRNA [63]. These findings indicate that the mechanism underlying the induction of avSGs and the viral RNA content of avSGs is dependent upon virus types. In any of these cases, however, avSGs play a critical role in the host antiviral IFN response. PKR is known to be essential for the formation of avSGs induced by NDV (Figure 3-13) and other viruses [56]. In measles virus (MeV) infection, PKR was shown to correlate

positively with both avSGs formation and IFN expression [77-79]. DHX36, another DExD/H-box helicase, has been shown to cooperate with PKR for the formation of avSGs and subsequent viral RNA sensing by RIG-I [59]. Pumilio proteins (PUM1 and 2) are known to cooperate with LGP2 to sense vRNA in order to trigger IFN-inducing signaling [80]. PKR, DHX36, and PUM1/2 are specifically recruited to avSGs. A critical signaling molecule for IFN induction, TRIM25, was shown to be specifically recruited to avSGs [59]. Taken together, these findings and the results from my study demonstrated that avSGs serve as a platform for the efficient sensing of viral RNA through the recruitment of antiviral molecules and critical signaling molecules.

4-4. The viral read-through transcripts; a novel natural ligand of RIG-I

In the last part of this study, I revealed that NDV, as well as other viruses belonging to *Mononegavirales* including RSV and VSV, produced Le-N/NS1 read-through RNA with 3'-poly(A) (Figure 3-22B, 3-24A, 3-25C, and F). The Le transcript has been shown to contain 5'-triphosphate [61, 81], and synthetic RNA corresponding to the Le-N activated *IFNB* gene (Figure 3-26A). These results strongly suggest that viral Le-N RNA synthesized within vRCs was transported to avSGs and detected by RIG-I. The generation of uncapped vRNA through transcriptional read-through is commonly found in other *Mononegavirales* viruses such as SeV, MeV, and VSV [68-70], suggesting that sensing of such uncapped viral RNA is an important strategy of antiviral innate immunity against these viruses. In the case of MeV, 5'-triphosphate Le RNA is considered to be a signature of activating RIG-I for IFN induction, and the association of RIG-I with the 5' end of the transcript covers the Le to N regions, corresponding to

the Le-N read-through transcript [82]. In future studies, it will be interesting to explore the general impact of an abortive Le-N read-through transcript, which is exclusively produced by viruses belonging to *Mononegavirales*, on the RIG-I-driven IFN pathway.

4-5. Conclusion

In this study, I intensively explored the association of RIG-I-driven antiviral IFN response with clusters of RNP complexes, vRCs and avSGs, in which potential RIG-I ligands exist. Although I entirely employed NDV for the most part in my experiments, I can suggest an important model to interpret the absolute function of RIG-I on the viral RNA detection and integration of the antiviral IFN response and stress response in the viral and host RNP complexes (Figure 4-1). The virus sensing in the cytoplasm involves more than simple interaction between sensor molecules and viral RNAs; a more complex mechanism, including various RNA binding proteins and stress response machinery, is responsible for detecting various viral RNA structures generated by the replication of different viruses. Thus, it will be interesting to investigate other types of viruses that deploy their own replication sites and avSGs to understand more about the fundamental role of RIG-I on the IFN response against viral infections.

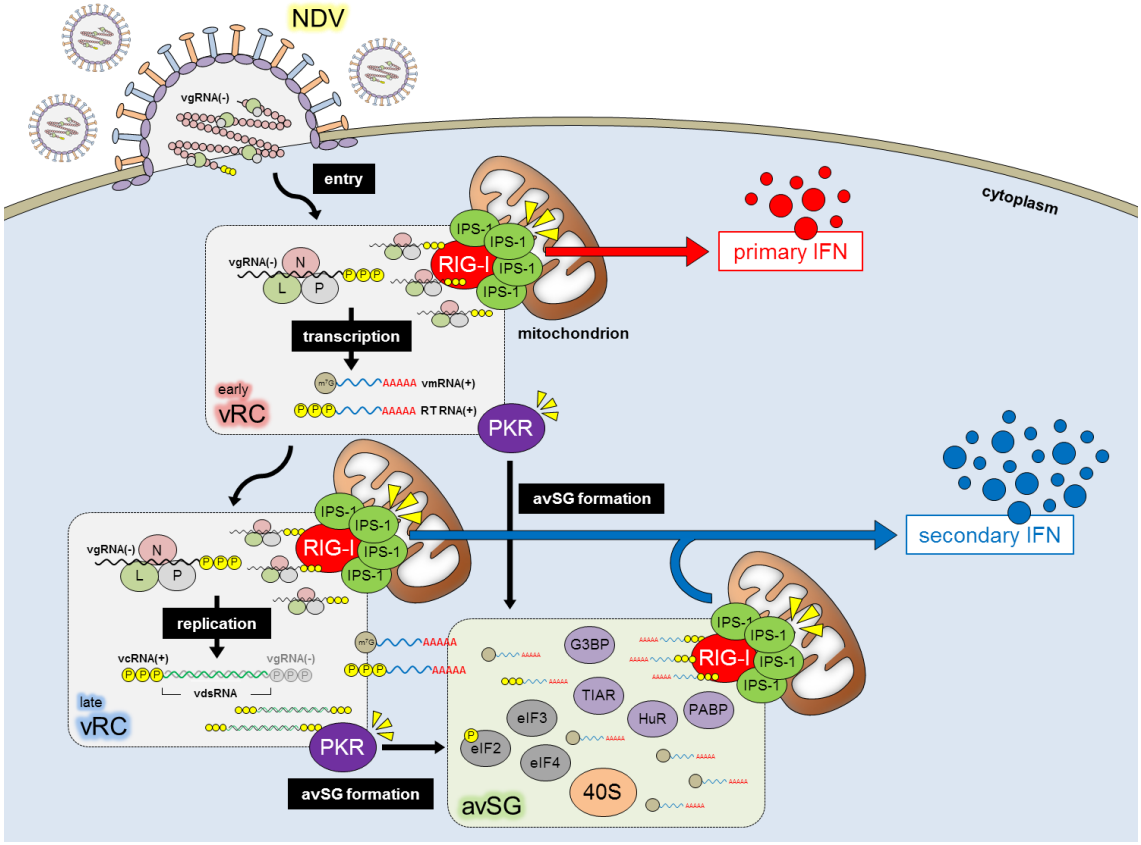

Figure 4-1. Kinetic model of NDV viral RNA sensing of RIG-I

NDV generates viral replication complexes (vRCs) in the early phase. RIG-I initially detects vgRNA(-) within early vRCs and induces primary IFN production in collaboration with IPS-1 aggregated around vRCs. At viral transcription, vmRNA and 5'-uncapped, 3'-polyadenylated read-through RNA (RT RNA) are produced. In the later phase, vdsRNA is produced as a replicative intermediate, forming the duplex of vgRNA(-) and vcRNA(+). PKR is activated by this product, or possibly by vgRNA or RT RNA with a double-strand in early vRCs. Once avSGs are induced, poly(A)-containing vmRNA and RT RNA are captured in avSGs, as well as host mRNAs. Subsequently, RIG-I accumulates in avSGs to detect 5'-uncapped RT RNA with IPS-1, and induce a secondary burst of IFN.

5. References

1. Kawai T, Akira S. The roles of TLRs, RLRs and NLRs in pathogen recognition. Int Immunol. 2009;21(4):317-37. doi: 10.1093/intimm/dxp017. PubMed PMID: 19246554; PubMed Central PMCID: PMCPMC2721684.

2. Thaiss CA, Levy M, Itav S, Elinav E. Integration of Innate Immune Signaling. Trends Immunol. 2016;37(2):84-101. doi: 10.1016/j.it.2015.12.003. PubMed PMID: 26755064.

3. Yoneyama M, Kikuchi M, Natsukawa T, Shinobu N, Imaizumi T, Miyagishi M, et al. The RNA helicase RIG-I has an essential function in double-stranded RNA-induced innate antiviral responses. Nat Immunol. 2004;5(7):730-7. doi: 10.1038/ni1087. PubMed PMID: 15208624.

4. Peisley A, Wu B, Xu H, Chen ZJ, Hur S. Structural basis for ubiquitin-mediated antiviral signal activation by RIG-I. Nature. 2014;509(7498):110-4. doi: 10.1038/nature13140. PubMed PMID: 24590070.

5. Jiang X, Kinch LN, Brautigam CA, Chen X, Du F, Grishin NV, et al. Ubiquitin-induced oligomerization of the RNA sensors RIG-I and MDA5 activates antiviral innate immune response. Immunity. 2012;36(6):959-73. doi: 10.1016/j.immuni.2012.03.022. PubMed PMID: 22705106; PubMed Central PMCID: PMCPMC3412146.

6. Gack MU, Shin YC, Joo CH, Urano T, Liang C, Sun L, et al. TRIM25 RING-finger E3 ubiquitin ligase is essential for RIG-I-mediated antiviral activity. Nature. 2007;446(7138):916-20. doi: 10.1038/nature05732. PubMed PMID: 17392790.

7. Kawai T, Takahashi K, Sato S, Coban C, Kumar H, Kato H, et al. IPS-1, an adaptor triggering RIG-I- and Mda5-mediated type I interferon induction. Nat Immunol.

2005;6(10):981-8. doi: 10.1038/ni1243. PubMed PMID: 16127453.

8. Seth RB, Sun L, Ea CK, Chen ZJ. Identification and characterization of MAVS, a mitochondrial antiviral signaling protein that activates NF-kappaB and IRF 3. Cell. 2005;122(5):669-82. doi: 10.1016/j.cell.2005.08.012. PubMed PMID: 16125763.

9. Xu LG, Wang YY, Han KJ, Li LY, Zhai Z, Shu HB. VISA is an adapter protein required for virus-triggered IFN-beta signaling. Mol Cell. 2005;19(6):727-40. doi: 10.1016/j.molcel.2005.08.014. PubMed PMID: 16153868.

10. Meylan E, Curran J, Hofmann K, Moradpour D, Binder M, Bartenschlager R, et al. Cardif is an adaptor protein in the RIG-I antiviral pathway and is targeted by hepatitis C virus. Nature. 2005;437(7062):1167-72. doi: 10.1038/nature04193. PubMed PMID: 16177806.

11. Hou F, Sun L, Zheng H, Skaug B, Jiang QX, Chen ZJ. MAVS forms functional prion-like aggregates to activate and propagate antiviral innate immune response. Cell. 2011;146(3):448-61. doi: 10.1016/j.cell.2011.06.041. PubMed PMID: 21782231; PubMed Central PMCID: PMCPMC3179916.

12. Onoguchi K, Onomoto K, Takamatsu S, Jogi M, Takemura A, Morimoto S, et al. Virus-infection or 5'ppp-RNA activates antiviral signal through redistribution of IPS-1 mediated by MFN1. PLoS Pathog. 2010;6(7):e1001012. doi: 10.1371/journal.ppat.1001012. PubMed PMID: 20661427; PubMed Central PMCID: PMCPMC2908619.

13. Saha SK, Pietras EM, He JQ, Kang JR, Liu SY, Oganesyan G, et al. Regulation of antiviral responses by a direct and specific interaction between TRAF3 and Cardif. EMBO J. 2006;25(14):3257-63. doi: 10.1038/sj.emboj.7601220. PubMed PMID: 16858409; PubMed Central PMCID: PMCPMC1523175.

14. Takahashi K, Kawai T, Kumar H, Sato S, Yonehara S, Akira S. Roles of caspase-8 and caspase-10 in innate immune responses to double-stranded RNA. J Immunol. 2006;176(8):4520-4. PubMed PMID: 16585540.

15. Michallet MC, Meylan E, Ermolaeva MA, Vazquez J, Rebsamen M, Curran J, et al. TRADD protein is an essential component of the RIG-like helicase antiviral pathway. Immunity. 2008;28(5):651-61. doi: 10.1016/j.immuni.2008.03.013. PubMed PMID: 18439848.

16. Pomerantz JL, Baltimore D. NF-kappaB activation by a signaling complex containing TRAF2, TANK and TBK1, a novel IKK-related kinase. EMBO J. 1999;18(23):6694-704. doi: 10.1093/emboj/18.23.6694. PubMed PMID: 10581243; PubMed Central PMCID: PMCPMC1171732.

17. Fitzgerald KA, McWhirter SM, Faia KL, Rowe DC, Latz E, Golenbock DT, et al. IKKepsilon and TBK1 are essential components of the IRF3 signaling pathway. Nat Immunol. 2003;4(5):491-6. doi: 10.1038/ni921. PubMed PMID: 12692549.

18. Chen ZJ, Parent L, Maniatis T. Site-specific phosphorylation of IkappaBalpha by a novel ubiquitination-dependent protein kinase activity. Cell. 1996;84(6):853-62. PubMed PMID: 8601309.

19. DiDonato JA, Hayakawa M, Rothwarf DM, Zandi E, Karin M. A cytokine-responsive IkappaB kinase that activates the transcription factor NF-kappaB. Nature. 1997;388(6642):548-54. doi: 10.1038/41493. PubMed PMID: 9252186.

20. Rothwarf DM, Zandi E, Natoli G, Karin M. IKK-gamma is an essential regulatory subunit of the IkappaB kinase complex. Nature. 1998;395(6699):297-300. doi: 10.1038/26261. PubMed PMID: 9751060.

21. Yamaoka S, Courtois G, Bessia C, Whiteside ST, Weil R, Agou F, et al.

Complementation cloning of NEMO, a component of the IkappaB kinase complex essential for NF-kappaB activation. Cell. 1998;93(7):1231-40. PubMed PMID: 9657155.

22. Mercurio F, Murray BW, Shevchenko A, Bennett BL, Young DB, Li JW, et al. IkappaB kinase (IKK)-associated protein 1, a common component of the heterogeneous IKK complex. Mol Cell Biol. 1999;19(2):1526-38. PubMed PMID: 9891086; PubMed Central PMCID: PMCPMC116081.

23. Onoguchi K, Yoneyama M, Takemura A, Akira S, Taniguchi T, Namiki H, et al. Viral infections activate types I and III interferon genes through a common mechanism. J Biol Chem. 2007;282(10):7576-81. doi: 10.1074/jbc.M608618200. PubMed PMID: 17204473.

24. Merika M, Williams AJ, Chen G, Collins T, Thanos D. Recruitment of CBP/p300 by the IFN beta enhanceosome is required for synergistic activation of transcription. Mol Cell. 1998;1(2):277-87. PubMed PMID: 9659924.

25. Yoneyama M, Kikuchi M, Matsumoto K, Imaizumi T, Miyagishi M, Taira K, et al. Shared and unique functions of the DExD/H-box helicases RIG-I, MDA5, and LGP2 in antiviral innate immunity. J Immunol. 2005;175(5):2851-8. PubMed PMID: 16116171.

26. Kato H, Sato S, Yoneyama M, Yamamoto M, Uematsu S, Matsui K, et al. Cell type-specific involvement of RIG-I in antiviral response. Immunity. 2005;23(1):19-28. doi: 10.1016/j.immuni.2005.04.010. PubMed PMID: 16039576.

27. Saito T, Owen DM, Jiang F, Marcotrigiano J, Gale M. Innate immunity induced by composition-dependent RIG-I recognition of hepatitis C virus RNA. Nature. 2008;454(7203):523-7. doi: 10.1038/nature07106. PubMed PMID: 18548002; PubMed Central PMCID: PMCPMC2856441.

28. Rehwinkel J, Tan CP, Goubau D, Schulz O, Pichlmair A, Bier K, et al. RIG-I detects viral genomic RNA during negative-strand RNA virus infection. Cell. 2010;140(3):397-408. doi: 10.1016/j.cell.2010.01.020. PubMed PMID: 20144762.

29. Kato H, Takeuchi O, Sato S, Yoneyama M, Yamamoto M, Matsui K, et al. Differential roles of MDA5 and RIG-I helicases in the recognition of RNA viruses. Nature. 2006;441(7089):101-5. doi: 10.1038/nature04734. PubMed PMID: 16625202.

30. Gitlin L, Barchet W, Gilfillan S, Cella M, Beutler B, Flavell RA, et al. Essential role of mda-5 in type I IFN responses to polyriboinosinic:polyribocytidylic acid and encephalomyocarditis picornavirus. Proc Natl Acad Sci U S A. 2006;103(22):8459-64. doi: 10.1073/pnas.0603082103. PubMed PMID: 16714379; PubMed Central PMCID: PMCPMC1464000.

31. Feng Q, Hato SV, Langereis MA, Zoll J, Virgen-Slane R, Peisley A, et al. MDA5 detects the double-stranded RNA replicative form in picornavirus-infected cells. Cell Rep. 2012;2(5):1187-96. doi: 10.1016/j.celrep.2012.10.005. PubMed PMID: 23142662.

32. Pichlmair A, Schulz O, Tan CP, Rehwinkel J, Kato H, Takeuchi O, et al. Activation of MDA5 requires higher-order RNA structures generated during virus infection. J Virol. 2009;83(20):10761-9. doi: 10.1128/JVI.00770-09. PubMed PMID: 19656871; PubMed Central PMCID: PMCPMC2753146.

33. Delaloye J, Roger T, Steiner-Tardivel QG, Le Roy D, Knaup Reymond M, Akira S, et al. Innate immune sensing of modified vaccinia virus Ankara (MVA) is mediated by TLR2-TLR6, MDA-5 and the NALP3 inflammasome. PLoS Pathog. 2009;5(6):e1000480. doi: 10.1371/journal.ppat.1000480. PubMed PMID: 19543380; PubMed Central PMCID: PMCPMC2691956.

34. Wang F, Gao X, Barrett JW, Shao Q, Bartee E, Mohamed MR, et al. RIG-I mediates

the co-induction of tumor necrosis factor and type I interferon elicited by myxoma virus in primary human macrophages. PLoS Pathog. 2008;4(7):e1000099. doi: 10.1371/journal.ppat.1000099. PubMed PMID: 18617992; PubMed Central PMCID: PMCPMC2438611.

35. Schulz O, Pichlmair A, Rehwinkel J, Rogers NC, Scheuner D, Kato H, et al. Protein kinase R contributes to immunity against specific viruses by regulating interferon mRNA integrity. Cell Host Microbe. 2010;7(5):354-61. doi: 10.1016/j.chom.2010.04.007. PubMed PMID: 20478537; PubMed Central PMCID: PMCPMC2919169.

36. Ikegame S, Takeda M, Ohno S, Nakatsu Y, Nakanishi Y, Yanagi Y. Both RIG-I and MDA5 RNA helicases contribute to the induction of alpha/beta interferon in measles virus-infected human cells. J Virol. 2010;84(1):372-9. doi: 10.1128/JVI.01690-09. PubMed PMID: 19846522; PubMed Central PMCID: PMCPMC2798399.

37. Loo YM, Fornek J, Crochet N, Bajwa G, Perwitasari O, Martinez-Sobrido L, et al. Distinct RIG-I and MDA5 signaling by RNA viruses in innate immunity. J Virol. 2008;82(1):335-45. doi: 10.1128/JVI.01080-07. PubMed PMID: 17942531; PubMed Central PMCID: PMCPMC2224404.

38. Fredericksen BL, Keller BC, Fornek J, Katze MG, Gale M. Establishment and maintenance of the innate antiviral response to West Nile Virus involves both RIG-I and MDA5 signaling through IPS-1. J Virol. 2008;82(2):609-16. doi: 10.1128/JVI.01305-07. PubMed PMID: 17977974; PubMed Central PMCID: PMCPMC2224571.

39. Kato H, Takeuchi O, Mikamo-Satoh E, Hirai R, Kawai T, Matsushita K, et al. Length-dependent recognition of double-stranded ribonucleic acids by retinoic acid-inducible gene-I and melanoma differentiation-associated gene 5. J Exp Med.

2008;205(7):1601-10. doi: 10.1084/jem.20080091. PubMed PMID: 18591409; PubMed Central PMCID: PMCPMC2442638.

40. Satoh T, Kato H, Kumagai Y, Yoneyama M, Sato S, Matsushita K, et al. LGP2 is a positive regulator of RIG-I- and MDA5-mediated antiviral responses. Proc Natl Acad Sci U S A. 2010;107(4):1512-7. doi: 10.1073/pnas.0912986107. PubMed PMID: 20080593; PubMed Central PMCID: PMCPMC2824407.

41. Hornung V, Ellegast J, Kim S, Brzózka K, Jung A, Kato H, et al. 5'-Triphosphate RNA is the ligand for RIG-I. Science. 2006;314(5801):994-7. doi: 10.1126/science.1132505. PubMed PMID: 17038590.

42. Flanegan JB, Petterson RF, Ambros V, Hewlett NJ, Baltimore D. Covalent linkage of a protein to a defined nucleotide sequence at the 5'-terminus of virion and replicative intermediate RNAs of poliovirus. Proc Natl Acad Sci U S A. 1977;74(3):961-5. PubMed PMID: 191841; PubMed Central PMCID: PMCPMC430548.

43. Lee YF, Nomoto A, Detjen BM, Wimmer E. A protein covalently linked to poliovirus genome RNA. Proc Natl Acad Sci U S A. 1977;74(1):59-63. PubMed PMID: 189316; PubMed Central PMCID: PMCPMC393196.

44. Schlee M, Roth A, Hornung V, Hagmann CA, Wimmenauer V, Barchet W, et al. Recognition of 5' triphosphate by RIG-I helicase requires short blunt double-stranded RNA as contained in panhandle of negative-strand virus. Immunity. 2009;31(1):25-34. doi: 10.1016/j.immuni.2009.05.008. PubMed PMID: 19576794; PubMed Central PMCID: PMCPMC2824854.

45. Schmidt A, Schwerd T, Hamm W, Hellmuth JC, Cui S, Wenzel M, et al. 5'-triphosphate RNA requires base-paired structures to activate antiviral signaling via RIG-I. Proc Natl Acad Sci U S A. 2009;106(29):12067-72. doi:

10.1073/pnas.0900971106. PubMed PMID: 19574455; PubMed Central PMCID: PMCPMC2705279.

46. Strähle L, Marq JB, Brini A, Hausmann S, Kolakofsky D, Garcin D. Activation of the beta interferon promoter by unnatural Sendai virus infection requires RIG-I and is inhibited by viral C proteins. J Virol. 2007;81(22):12227-37. doi: 10.1128/JVI.01300-07. PubMed PMID: 17804509; PubMed Central PMCID: PMCPMC2169027.

47. Weber F, Wagner V, Rasmussen SB, Hartmann R, Paludan SR. Double-stranded RNA is produced by positive-strand RNA viruses and DNA viruses but not in detectable amounts by negative-strand RNA viruses. J Virol. 2006;80(10):5059-64. doi: 10.1128/JVI.80.10.5059-5064.2006. PubMed PMID: 16641297; PubMed Central PMCID: PMCPMC1472073.

48. Zhang S, Sun Y, Chen H, Dai Y, Zhan Y, Yu S, et al. Activation of the PKR/eIF2α signaling cascade inhibits replication of Newcastle disease virus. Virol J. 2014;11:62. doi: 10.1186/1743-422X-11-62. PubMed PMID: 24684861; PubMed Central PMCID: PMCPMC3994276.

49. Goubau D, Schlee M, Deddouche S, Pruijssers AJ, Zillinger T, Goldeck M, et al. Antiviral immunity via RIG-I-mediated recognition of RNA bearing 5'-diphosphates. Nature. 2014;514(7522):372-5. doi: 10.1038/nature13590. PubMed PMID: 25119032; PubMed Central PMCID: PMCPMC4201573.

50. Davis WG, Bowzard JB, Sharma SD, Wiens ME, Ranjan P, Gangappa S, et al. The 3' untranslated regions of influenza genomic sequences are 5'PPP-independent ligands for RIG-I. PLoS One. 2012;7(3):e32661. doi: 10.1371/journal.pone.0032661. PubMed PMID: 22438882; PubMed Central PMCID: PMCPMC3305289.

51. Kedersha NL, Gupta M, Li W, Miller I, Anderson P. RNA-binding proteins TIA-1

and TIAR link the phosphorylation of eIF-2 alpha to the assembly of mammalian stress granules. J Cell Biol. 1999;147(7):1431-42. PubMed PMID: 10613902; PubMed Central PMCID: PMCPMC2174242.

52. Gallouzi IE, Brennan CM, Stenberg MG, Swanson MS, Eversole A, Maizels N, et al. HuR binding to cytoplasmic mRNA is perturbed by heat shock. Proc Natl Acad Sci U S A. 2000;97(7):3073-8. PubMed PMID: 10737787; PubMed Central PMCID: PMCPMC16194.

53. Kedersha N, Chen S, Gilks N, Li W, Miller IJ, Stahl J, et al. Evidence that ternary complex (eIF2-GTP-tRNA(i)(Met))-deficient preinitiation complexes are core constituents of mammalian stress granules. Mol Biol Cell. 2002;13(1):195-210. doi: 10.1091/mbc.01-05-0221. PubMed PMID: 11809833; PubMed Central PMCID: PMCPMC65082.

54. Kimball SR, Horetsky RL, Ron D, Jefferson LS, Harding HP. Mammalian stress granules represent sites of accumulation of stalled translation initiation complexes. Am J Physiol Cell Physiol. 2003;284(2):C273-84. doi: 10.1152/ajpcell.00314.2002. PubMed PMID: 12388085.

55. Tourrière H, Chebli K, Zekri L, Courselaud B, Blanchard JM, Bertrand E, et al. The RasGAP-associated endoribonuclease G3BP assembles stress granules. J Cell Biol. 2003;160(6):823-31. doi: 10.1083/jcb.200212128. PubMed PMID: 12642610; PubMed Central PMCID: PMCPMC2173781.

56. Onomoto K, Yoneyama M, Fung G, Kato H, Fujita T. Antiviral innate immunity and stress granule responses. Trends Immunol. 2014;35(9):420-8. doi: 10.1016/j.it.2014.07.006. PubMed PMID: 25153707.

57. García MA, Meurs EF, Esteban M. The dsRNA protein kinase PKR: virus and cell

control. Biochimie. 2007;89(6-7):799-811. doi: 10.1016/j.biochi.2007.03.001. PubMed PMID: 17451862.

58. Onomoto K, Jogi M, Yoo JS, Narita R, Morimoto S, Takemura A, et al. Critical role of an antiviral stress granule containing RIG-I and PKR in viral detection and innate immunity. PLoS One. 2012;7(8):e43031. doi: 10.1371/journal.pone.0043031. PubMed PMID: 22912779; PubMed Central PMCID: PMCPMC3418241.

59. Yoo JS, Takahasi K, Ng CS, Ouda R, Onomoto K, Yoneyama M, et al. DHX36 enhances RIG-I signaling by facilitating PKR-mediated antiviral stress granule formation. PLoS Pathog. 2014;10(3):e1004012. doi: 10.1371/journal.ppat.1004012. PubMed PMID: 24651521; PubMed Central PMCID: PMCPMC3961341.

60. Lamb RA, Parks GD. *Paramyxoviridae*: The Viruses and Their Replication. In: Knipe DM, Howley PM, editors. Fields Virology. 1. 5 ed. Philadelphia: Wolters Kluwer Health/Lippincott Williams & Wilkins; 2007. p. 1449-96.

61. Colonno RJ, Banerjee AK. A unique RNA species involved in initiation of vesicular stomatitis virus RNA transcription in vitro. Cell. 1976;8(2):197-204. PubMed PMID: 183891.

62. Lamb RA. *Mononegavirales*. In: Knipe DM, Howley PM, editors. Fields virology. 5 ed. Philadelphia: Wolters Kluwer Health/Lippincott Williams & Wilkins; 2007. p. 1357-61.

63. Ng CS, Jogi M, Yoo JS, Onomoto K, Koike S, Iwasaki T, et al. Encephalomyocarditis virus disrupts stress granules, the critical platform for triggering antiviral innate immune responses. J Virol. 2013;87(17):9511-22. doi: 10.1128/JVI.03248-12. PubMed PMID: 23785203; PubMed Central PMCID: PMCPMC3754122.

64. Takahasi K, Yoneyama M, Nishihori T, Hirai R, Kumeta H, Narita R, et al. Nonself RNA-sensing mechanism of RIG-I helicase and activation of antiviral immune responses. Mol Cell. 2008;29(4):428-40. doi: 10.1016/j.molcel.2007.11.028. PubMed PMID: 18242112.

65. Kawakami E, Watanabe T, Fujii K, Goto H, Watanabe S, Noda T, et al. Strand-specific real-time RT-PCR for distinguishing influenza vRNA, cRNA, and mRNA. J Virol Methods. 2011;173(1):1-6. doi: 10.1016/j.jviromet.2010.12.014. PubMed PMID: 21185869; PubMed Central PMCID: PMCPMC3049850.

66. Matsuki H, Takahashi M, Higuchi M, Makokha GN, Oie M, Fujii M. Both G3BP1 and G3BP2 contribute to stress granule formation. Genes Cells. 2013;18(2):135-46. doi: 10.1111/gtc.12023. PubMed PMID: 23279204.

67. Yan Y, Samal SK. Role of intergenic sequences in newcastle disease virus RNA transcription and pathogenesis. J Virol. 2008;82(3):1323-31. doi: 10.1128/JVI.01989-07. PubMed PMID: 18032502; PubMed Central PMCID: PMCPMC2224428.

68. Herman RC, Schubert M, Keene JD, Lazzarini RA. Polycistronic vesicular stomatitis virus RNA transcripts. Proc Natl Acad Sci U S A. 1980;77(8):4662-5. PubMed PMID: 6254036; PubMed Central PMCID: PMCPMC349905.

69. Vidal S, Kolakofsky D. Modified model for the switch from Sendai virus transcription to replication. J Virol. 1989;63(5):1951-8. PubMed PMID: 2539496; PubMed Central PMCID: PMCPMC250608.

70. Plumet S, Duprex WP, Gerlier D. Dynamics of viral RNA synthesis during measles virus infection. J Virol. 2005;79(11):6900-8. doi: 10.1128/JVI.79.11.6900-6908.2005. PubMed PMID: 15890929; PubMed Central PMCID: PMCPMC1112129.

71. Tang ED, Wang CY. MAVS self-association mediates antiviral innate immune

signaling. J Virol. 2009;83(8):3420-8. doi: 10.1128/JVI.02623-08. PubMed PMID: 19193783; PubMed Central PMCID: PMCPMC2663242.

72. Pichlmair A, Schulz O, Tan CP, Näslund TI, Liljeström P, Weber F, et al. RIG-I-mediated antiviral responses to single-stranded RNA bearing 5'-phosphates. Science. 2006;314(5801):997-1001. doi: 10.1126/science.1132998. PubMed PMID: 17038589.

73. Weber M, Gawanbacht A, Habjan M, Rang A, Borner C, Schmidt AM, et al. Incoming RNA virus nucleocapsids containing a 5'-triphosphorylated genome activate RIG-I and antiviral signaling. Cell Host Microbe. 2013;13(3):336-46. doi: 10.1016/j.chom.2013.01.012. PubMed PMID: 23498958.

74. Buchan JR, Parker R. Eukaryotic stress granules: the ins and outs of translation. Mol Cell. 2009;36(6):932-41. doi: 10.1016/j.molcel.2009.11.020. PubMed PMID: 20064460; PubMed Central PMCID: PMCPMC2813218.

75. Daffis S, Szretter KJ, Schriewer J, Li J, Youn S, Errett J, et al. 2'-O methylation of the viral mRNA cap evades host restriction by IFIT family members. Nature. 2010;468(7322):452-6. doi: 10.1038/nature09489. PubMed PMID: 21085181; PubMed Central PMCID: PMCPMC3058805.

76. Schuberth-Wagner C, Ludwig J, Bruder AK, Herzner AM, Zillinger T, Goldeck M, et al. A Conserved Histidine in the RNA Sensor RIG-I Controls Immune Tolerance to N-2'O-Methylated Self RNA. Immunity. 2015. Epub 2015/07/19. doi: 10.1016/j.immuni.2015.06.015. PubMed PMID: 26187414.

77. McAllister CS, Toth AM, Zhang P, Devaux P, Cattaneo R, Samuel CE. Mechanisms of protein kinase PKR-mediated amplification of beta interferon induction by C protein-deficient measles virus. J Virol. 2010;84(1):380-6. doi: 10.1128/JVI.02630-08.

PubMed PMID: 19846517; PubMed Central PMCID: PMCPMC2798421.

78. Li Z, Okonski KM, Samuel CE. Adenosine deaminase acting on RNA 1 (ADAR1) suppresses the induction of interferon by measles virus. J Virol. 2012;86(7):3787-94. doi: 10.1128/JVI.06307-11. PubMed PMID: 22278222; PubMed Central PMCID: PMCPMC3302501.

79. Okonski KM, Samuel CE. Stress granule formation induced by measles virus is protein kinase PKR dependent and impaired by RNA adenosine deaminase ADAR1. J Virol. 2013;87(2):756-66. doi: 10.1128/JVI.02270-12. PubMed PMID: 23115276; PubMed Central PMCID: PMCPMC3554044.

80. Narita R, Takahasi K, Murakami E, Hirano E, Yamamoto SP, Yoneyama M, et al. A novel function of human Pumilio proteins in cytoplasmic sensing of viral infection. PLoS Pathog. 2014;10(10):e1004417. doi: 10.1371/journal.ppat.1004417. PubMed PMID: 25340845; PubMed Central PMCID: PMCPMC4207803.

81. Plumet S, Herschke F, Bourhis JM, Valentin H, Longhi S, Gerlier D. Cytosolic 5'-triphosphate ended viral leader transcript of measles virus as activator of the RIG I-mediated interferon response. PLoS One. 2007;2(3):e279. doi: 10.1371/journal.pone.0000279. PubMed PMID: 17356690; PubMed Central PMCID: PMCPMC1804102.

82. Runge S, Sparrer KM, Lässig C, Hembach K, Baum A, García-Sastre A, et al. In vivo ligands of MDA5 and RIG-I in measles virus-infected cells. PLoS Pathog. 2014;10(4):e1004081. doi: 10.1371/journal.ppat.1004081. PubMed PMID: 24743923; PubMed Central PMCID: PMCPMC3990713.

6. Acknowledgements

Firstly, I would like to express my sincere gratitude to my advisor Prof. *Takashi Fujita* for his continuous support of my Ph.D. studies, for his patience, motivation, and immense knowledge. His guidance helped me at all times during my research. As well as my advisor, I would like to thank Assoc. Prof. *Hiroki Kato* for his insightful comments and encouragement, and also for his strict guidance which incented me to widen my research to consider perspectives. My sincere thanks also goes to Prof. *Mitsutoshi Yoneyama*, Dr. *Koji Onomoto*, and Dr. *Kazuhide Onoguchi*; their advice on both my research as well as on my career has been priceless. I would also especially like to thank Assoc. Prof. *Takahiro Fujiwara* and Dr. *Fumiyoshi Ishidate* for the exciting work on the imaging experiments. I thank my lab members for the stimulating discussions, for the hard-working sleepless nights, and for all the fun moments we have shared together.

A special thanks to my family. Words cannot express how grateful I am to my father, my mother, my sister, and my wife. All of your supports, sacrifices, encouragements, and love offered mental and spiritual sustenance for me.

This thesis was written based on the following original article;

Seong-Wook Oh, Koji Onomoto, Mai Wakimoto, Kazuhide Onoguchi, Fumiyoshi Ishidate, Takahiro Fujiwara, Mitsutoshi Yoneyama, Hiroki Kato, and Takashi Fujita

"Leader-Containing Uncapped Viral Transcript Activates RIG-I in Antiviral Stress Granules"

PLOS Pathogens 12(2), e1005444 (2016)